BRNO UNIVERSITY OF TECHNOLOGY
VYSOKÉ UČENÍ TECHNICKÉ V BRNĚ

FACULTY OF INFORMATION TECHNOLOGY
FAKULTA INFORMAČNÍCH TECHNOLOGIÍ

DEPARTMENT OF COMPUTER GRAPHICS AND MULTIMEDIA
ÚSTAV POČÍTAČOVÉ GRAFIKY A MULTIMÉDIÍ

RADAR SIGNAL PROCESSING FOR RADIO ALTIMETER

ZPRACOVÁNÍ RADAROVÉHO SIGNÁLU PRO RÁDIOVÝ VÝŠKOMĚR

MASTER'S THESIS
DIPLOMOVÁ PRÁCE

AUTHOR **Bc. MILAN KRASŇANSKÝ**
AUTOR PRÁCE

SUPERVISOR **prof. Dr. Ing. PAVEL ZEMČÍK**
VEDOUCÍ PRÁCE

BRNO 2017

Master's Thesis Specification/17508/2016/xkrasn06

Brno University of Technology - Faculty of Information Technology

Department of Computer Graphics and Multimedia Academic year 2016/2017

Master's Thesis Specification

For: **Krasňanský Milan, Bc.**
Branch of study: Computer Graphics and Multimedia
Title: **Radar Signal Processing for Radio Altimeter**
Category: Singal Processing

Instructions for project work:

1. Study the available sources of information about altimeters for light aircraft and algorithms for Doppler radar modulation and signal processing as well as tools for signal processing.
2. Select or propose a suitable method of Doppler radar modulation and signal processing for light aircraft with focus on real-time capability of the algorithm.
3. Propose a method of implementation for a selected target embedded platform and discuss the achievable features.
4. Implement the algorithm and demonstrate its functionality on a set of signals. The algorithm does not necessarily have to be implemented in an embedded system but it can be simulated on a PC using a suitable signal processing tool.
5. Discuss the results of the project and possible future work.

Basic references:

- According to the supervisor's instruction

Requirements for the semestral defense:

- Items 1-3 of the assignment

Detailed formal specifications can be found at http://www.fit.vutbr.cz/info/szz/

The Master's Thesis must define its purpose, describe a current state of the art, introduce the theoretical and technical background relevant to the problems solved, and specify what parts have been used from earlier projects or have been taken over from other sources.

Each student will hand-in printed as well as electronic versions of the technical report, an electronic version of the complete program documentation, program source files, and a functional hardware prototype sample if desired. The information in electronic form will be stored on a standard non-rewritable medium (CD-R, DVD-R, etc.) in formats common at the FIT. In order to allow regular handling, the medium will be securely attached to the printed report.

Supervisor: **Zemčík Pavel, prof. Dr. Ing.**, DCGM FIT BUT
Beginning of work: November 1, 2016
Date of delivery: May 24, 2017

VYSOKÉ UČENÍ TECHNICKÉ V BRNĚ
Fakulta informačních technologií
Ústav počítačové grafiky a multimédií
612 66 Brno, Božetěchova 2

L.S.

Jan Černocký
Associate Professor and Head of Department

Abstract

This diploma thesis deals with designing and implementation of an algorithm for frequency–modulated continuous–wave radar signal processing. The goal is to implement an algorithm, which would be sufficiently fast (real–time capability on the target platform) and sufficiently accurate for its usage in the radio altimeter in the light aircraft, especially during the landing manoeuvre. The main signal processing method used in the implementation is the Discrete Fourier Transform. The created algorithm has been tested on the real flight data and achieved satisfactory results for the landing manoeuvre.

Abstrakt

Táto diplomová práca sa zaoberá návrhom a implementáciou algoritmu pre spracovaniu signálu z radaru využívajúceho frekvenčne modulovanú kontinuálnu vlnu. Cieľom je implementácia algoritmu, ktorý by bol dostatočne rýchly (výpočet v reálnom čase na cieľovej platforme) a dostatočne presný pre použitie v rádiovýškomere v ľahkom lietadle so zameraním na použitie počas pristávacieho manévru. Hlavnou metódou spracovania signálu, použitou v implementácii, je Diskrétna Fourierova transformácia. Vytvorený algoritmus bol otestovaný na reálnych letových dátach a pre pristávací manéver dosiahol uspokojivé výsledky.

Keywords

signal processing, frequency modulation, radar, radio altimeter, discrete Fourier transform

Klíčová slova

spracovanie signálu, frekvenčná modulácia, radar, rádiovýškomer, diskrétna Fourierova transformácia

Reference

KRASŇANSKÝ, Milan. *Radar Signal Processing for Radio Altimeter*. Brno, 2017. Master's thesis. Brno University of Technology, Faculty of Information Technology. Supervisor Zemčík Pavel.

Rozšířený abstrakt

Cieľom tejto diplomovej práce je navrhnúť a implementovať algoritmus pre spracovanie radarového signálu, ktorý by mohol byť použitý v rádiovýškomere pre ľahké lietadlo, určenom predovšetkým na použitie počas pristávacieho manévru.

V úvode práca podáva stručný prehľad súčasného stavu v zariadeniach pre meranie výšky v letectve (rádiovýškomer, barometrický výškomer, satelitné navigácie) a uvádza popis princípu ich činnosti a približné parametre, ktoré tieto zariadenia dosahujú.

Ďalej je popisaný detailne pristávací manéver ľahkého športového lietadla a práca uvádza teoretické minimum o rôznych typoch radarov, rôznych typoch frekvenčných modulácii (a stručné porovnanie najpoužívanejších) a spracovaní radarového signálu s využitím jednodimenzionálnej aj dvojdimenzionálnej Diskrétnej Fourierovej transformácie na získanie informácie o výške lietadla a jeho vertikálnej rýchlosti ako aj číslicovom spracovaní a predspracovaní signálov ako takom.

Na základe týchto informácii je prezentovaný návrh riešenia s popisom uvažovanej cieľovej platformy, použitých prostriedkov a požadovaných parametrov výsledného riešenia s následným detailným popisom implementácie v prostredí softvéru Matlab, pričom riešenie je založené predovšetkým na využití jednodimenzionálnej Diskrétnej Fourierovej transformácii a signálu s trojuholníkovou frekvenčnou moduláciou. Súčasťou popisu riešenia sú tiež metódy, ktoré boli vytvorené pre zlepšenie detekcie v dátach obsahujúcich šum.

Záver práce tvorí popis a zhodnotenie dosiahnutých výsledkov vo forme výškových priebehov z letov ľahkého lietadla a následné naznačenie ďalších vylepšení algoritmu či ďalšieho smerovania práce. Vytvorený algoritmus bol otestovaný na reálnych letových dátach a pre pristávací manéver dosiahol uspokojivé výsledky.

Radar Signal Processing for Radio Altimeter

Declaration

Hereby I declare that this Master's thesis was prepared as an original author's work under the supervision of prof. Dr. Ing. Pavel Zemčík. All the relevant information sources, which were used during preparation of this thesis, are properly cited and included in the list of references.

.....
Milan Krasňanský
May 23, 2017

Acknowledgements

I would like to express my gratitude towards prof. Dr. Ing. Pavel Zemčík for his invaluable expert advice, patience, exemplary pedagogical approach combining the right amount of freedom and pressure and a considerable amount of time spent on consultations.

Contents

Chapter 1

Introduction

Since the first flight of the Wright Flyer back in 1903, airplanes, as well as other flying vehicles, have been an important part of our society, even though they were first seen as a hobby of a few enthusiasts. People quickly realized their potential and started using them for all thinkable purposes, which led to the rapid development of aviation. Nowadays, aircraft provide convenient and fast mean of transport for both passengers and cargo, and are also used in sport, research or serve in armed forces.

This rapid development led to the same situation as the rapid development of car transportation: an increased number of accidents. Some of the accidents can be attributed to the technical failure, poor weather conditions, an error in the fundamental design of the particular aircraft or human error, because humans, after all, make mistakes, be it an experienced factory test pilot or an enthusiast on a weekend flight.

Statistically, one of the most dangerous situation that can happen during the flight is the one which happens on every flight: a landing. The landing manoeuvre combines two phenomenons which are potentially dangerous alone, let alone combined. They are the close proximity of the ground and low speed. Therefore, in the past decades, many devices, whether installed on the aircraft or not, were designed to help the pilot fly safely at altitude and bring the aircraft safely to the ground: basic flight instruments (airspeed indicator, pressure altimeter, vertical speed indicator, attitude indicator, compass and others) as well as navigational systems such as VOR, NDB or Instrument Landing System.

Many of small and light aircraft are, however, unequipped for using Instrument Landing System, or, even if they are, they often land at airfields or airstrips, which do not provide support for such systems. These aircraft are, of course, seldom used in low–visibility situation but one difficulty remains and that is the height above the ground estimation.

One of the possible solutions to this problem is the usage of the radio altimeter. The radio altimeter as such is not a new device. The first usage dates back to the Second World War, when it was used in the automatic pull–up device, which dive bombers were equipped with. Since then, it made its way into the civil aviation and it is the standard equipment of most bigger, commercially used airplanes, but it is yet to be widely used in general aviation.

The advantages of utilizing the radio altimeter as additional safety enhancing device during the landing manoeuvre are especially the accuracy of the measured height, no significant delay of the height measurement and no need for height calibration (pressure altimeters would require setting the zero height which requires the knowledge of the current atmospheric pressure at the desired landing location which is often an unavailable information). Apart from the height measurement, the radio altimeter can also provide the pilot with the information about the vertical speed.

Therefore, the usage of radio altimeters in general aviation can be expected to become more common in the future. The aim of this Master's thesis is to contribute to the widespread use of this safety–enhancing device.

The goal is to the design and implement an algorithm, capable of being computed in the real time on commercially available and affordable embedded systems (or Systems–on–chip) while maintaining the sufficient accuracy.

This diploma thesis is divided into several chapters. The second chapter 2 provides the description of currently used height (or altitude) measurement devices and detailed description of the landing manoeuvre of the light airplane. The third chapter 3 describes the radar, the Doppler effect, frequency–modulated continuous–wave radars and signal processing of FMCW radar signals. The fourth chapter 4 deals with the digital signal processing in general and provides the description of basic techniques and methods of the signal processing. The fifth chapter 5 provides the proposal of the solution and brief description of the used software and possible target platforms. The next chapter 6 is aimed at detailed description of the designed and implement algorithm. Both the implementation and reasons for such solutions are provided to the reader. The chapter 7 shows and discusses the achieved results and tries to evaluate them. The chapter number 8 is aimed at possible improvements and the future of this project or possible related projects. The thesis is concluded by chapter 9 which provides the summary and the general conclusion.

Chapter 2

Aicraft altimeter and its usage for landing

As this thesis deals with designing a radar altimeter for an airplane, this chapter provides a description of the radio altimeter and also a description of a pressure altimeter, which is the primary altitude or height measuring device in most aircraft today. It is worth mentioning that altitude can be measured also by using satellite navigation systems such as GPS/NAVSTAR, Galileo or GLONASS and, during the Golden Age of Aviation in 1931, a sonic altimeter has been tested [1].

The aim of this chapter is to provide the reader with the overview of the thesis related facts about the the state–of–the–art approaches to the height/altitude measurement in the modern aviation with the focus on altimeters. Even though it may not be obvious at first glance, most of the following devices utilize information technology in some manner. The radio altimeter, of course, utilizes the digital signal processing, satellite navigation systems need to process the signal as well and also compute the position, not to mention the software used in the actual on–orbit satellites. Probably the least IT device as such in this overview is the pressure altimeter, but it is the primary height–measuring device today and it is also mentioned for completeness sake.

2.1 Pressure altimeter

The pressure altimeter is a pressure gauge calibrated to measure and indicate the height. The height is determined by the weight of an air column which extends vertically from the point of measurement to the outer atmosphere. This is called a static pressure and, apart from measuring the height, is also used to indicate the vertical speed (variometer). The higher the aircraft flies, the shorter (and thus lighter) is the air column which subsequently induces less pressure on the aircraft where it is measured by pressure heads [4].

It should be also noted that the aircraft is also subject to dynamic pressure, which is a consequence of the resistance of the air as the aircraft travels through it at a non-zero speed. Leading edges of the aircraft are therefore subject to both static and dynamic pressure which together are called total pressure or pitot pressure [4].

These two physical quantities are measured by pressure heads mounted on the outside of the aircraft, usually at the nose of the aircraft or at the leading edge of the wing (see figure 2.1). Inside a pressure head, there is a tube which, in case of measuring pitot pressure, has forward end open facing the oncoming airstream and the other end leads to the airspeed

capsules and machmeter. The moving airstream is brought to a rest, generating additional pressure which together with static pressure accounts for a total pressure.

Static pressure tube does not have an open forward end, but it has holes or slots on its sides which do not face the oncoming airstream and therefore measure only static pressure [4].

The head for the pitot and static may be combined (a head contains both tubes, see figure 2.2) two measure both quantities, creating pitot/static pressure head, sometimes referred to as „pitot/static tube“ [4].

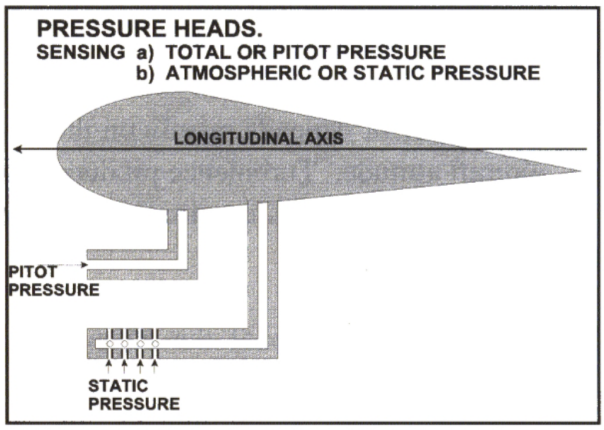

Figure 2.1: Dedicated pressure heads and their position at the leading edge of the wing [4]

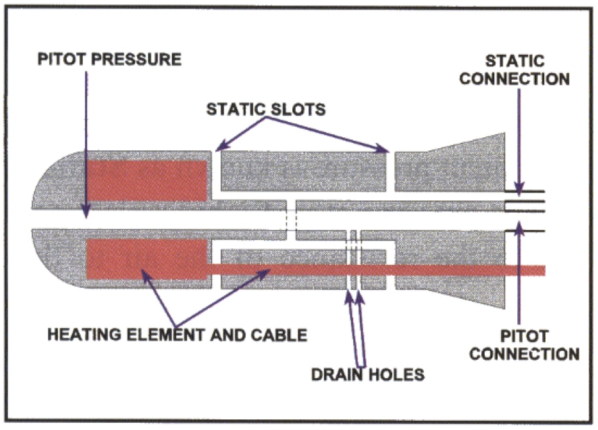

Figure 2.2: Detail of the combined pressure head [4]

Unfortunately, the relationship between the weight of the air column and the altitude (or the height) is not linear [4], so a calibration of the altimeter is needed, which is usually done using International Standard Atmosphere [2].

Today, two types of pressure altimeters exist. A simple altimeter and so called sensitive altimeter. In the simple altimeter, a static pressure is brought into the case of the instrument. As the pressure decreases, a capsule controlled by a leaf spring expands. This expansion is converted to the rotational movement of a single pointer via mechanical linkage. This mechanical linkage also incorporates the temperature-compensation device to

compensate for the expansion and the contraction of the mechanism due to the temperature change [4]. A simple pressure altimeter is shown in the figure 2.3. Altimeter also

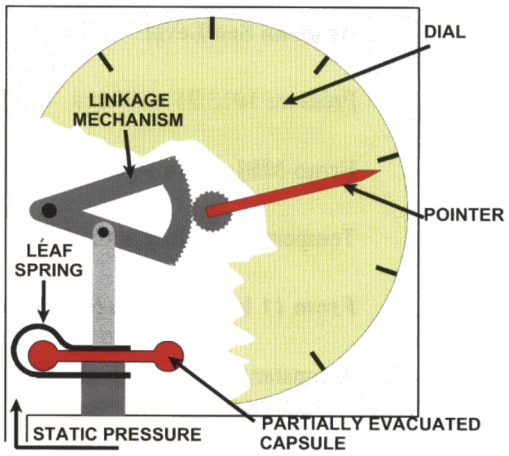

Figure 2.3: A simple pressure altimeter [4]

contains a setting knob, which can be used to set the altimeter zero with the aircraft on the ground (and thus showing the height above the ground (or, to be more precise, height above the airport ground) or to be set to the airport elevation (and thus showing height above the mean sea level) [4].

However, today, most aircraft are equipped with sensitive altimeter, which is also called „three - pointer“. The principle of construction is similar, but the sensitive type has two or three capsules to drive three pointers, geared 100:10:1, thus showing 100 ,000 feet per revolution, 10 ,000 feet per revolution and 1 ,000 feet per revolution [1]. The sensitive altimeter also has jewelled bearings to reduce friction and variable datum mechanism, so that the pilot can set the altimeter to show the height above any given pressure datum [4]. Schematics of the construction of sensitive altimeter is shown in figure 2.4. It should be also noted that current instruments are also usually servo-assisted to increase the operational range and also to increase the accuracy [4].

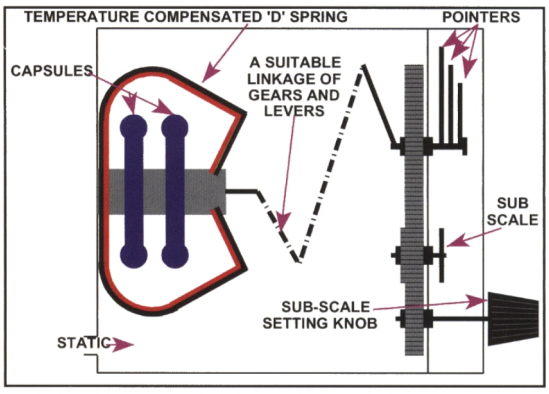

Figure 2.4: A sensitive pressure altimeter [4]

[1] Aviation instruments are usually calibrated in imperial units, not metric - feet is used for the altitude (height), knots for airspeed, a distance is usually given in nautical miles.

Tolerances and errors of pressure altimeters

Typical tolerances for pressure altimeters are [4]: 100 feet at the zero height and 1,000 feet at 35,000 feet for simple altimeter; 70 feet at the zero height and 600 feet at 40,000 feet for sensitive altimeter and 30 feet and 100 feet at the zero height and at 40,000 feet for servo-assisted altimeter.

Pressure altimeters are also subject to errors such as the time lag which causes the altimeter to under-read during climb and over-read during descent, the barometric error (local pressure has changed since the altimeter was set), the manoeuvre-induced error (pressure fluctuations when aircraft changes attitude, mainly the pitch attitude), temperature error (when real conditions differ from standard atmosphere; for example, in the colder air, the altimeter will over-read), the position error (inability to sense true static pressure) or instrument errors (the friction in the mechanism, manufacture imperfections) [4].

2.2 Radio altimeter

The radio altimeter is a device capable of measuring height of the aircraft above the ground with the high degree of accuracy. However, its function is not only to provide the crew with this information, but it also provides the data to two important systems in modern aircraft: the automatic flight system when used with instrument or microwave landing system and the ground proximity warning system where it also supplies the rate of change of the height [4].

As the name suggests, this instrument utilizes primary radar, transmitting frequency–modulated continuous–wave vertically below the aircraft.

The radio altimeter determines the time taken for a transmitted radio wave to travel to the ground directly beneath the aircraft and back again to the receiver on the aircraft. During this time the radio wave varies in the frequency up and down at a known rate over a fixed period of time by the frequency modulation completing the modulation cycle (an example is shown in the figure 2.5) [4].

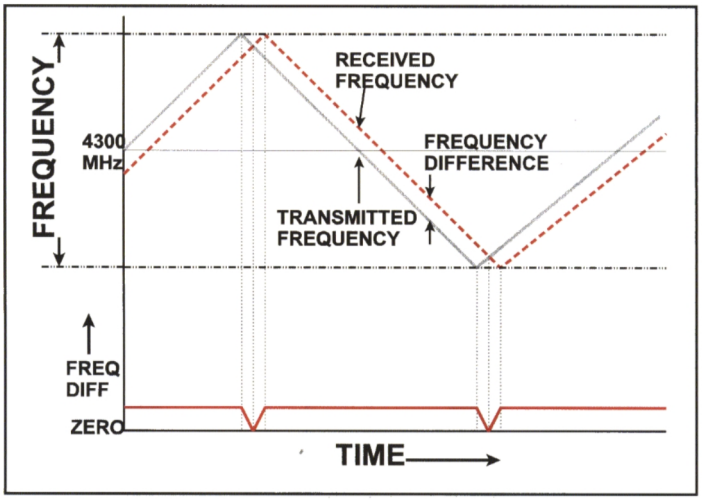

Figure 2.5: The modulation cycle [4]

The instrument compares frequencies of transmitted and received signals and using the known rate of change, it computes the time taken for the radio wave to travel from the

aircraft to the ground and back to the aircraft from the frequency difference. The computed time is then used to compute the distance to the ground or, in other words, the height of the aircraft above the ground [4].

When the transmitter changes the direction of its frequency sweep, the breakdown of frequency difference occurs which is overcome by relating the aircraft height to the average beat frequency observed over a short sampling period. The frequency changeover points are therefore ignored [4].

2.3 Satellite systems

Another mean to determine the altitude is to use satellite navigation systems. As of today (2016-23-12), two global navigation systems are fully operational (GPS/NAVSTAR operated by the USA and GLONASS operated by the Russian Federation) [5] and third (Galileo operated by the European Union) has only recently been released for general public use (albeit currently only for smartphones and built-in car navigation systems and should be fully operational by 2020 [11].

These systems use signals from satellites orbiting the Earth to triangulate the position of the receiver. To determine so called 3D fix (the latitude, the longitude and the altitude), 4 visible satellites are needed (and for reasonable accuracy one of them should be near the vertical overhead position) [12]. The horizontal accuracy of these systems is currently well under 5 meters [5] and the vertical accuracy is 10 to 20 meters [12].

2.4 Landing manoeuvre

The landing manoeuvre of an airplane consists of several phases. Airplane Flying Handbook published by Federal Aviation Authority of U.S. Department of Transportation describes these [8]:

1. the base leg (of the airfield traffic pattern)
2. the final approach
3. the round out (flare)
4. the touchdown
5. the after–landing roll

It is worth mentioning that some other publications, such as Učebnice Sportovního Letce by František Kédr et al. [15] divides round out into two separate phases, but the principle is the same. For the purpose of this thesis, only phases 2, 3 and 4 will be described.

The final approach

The final approach begins when the airplane completes the base–to–final turn (see the figure 2.6) of the airfield traffic pattern (the path of movement of the aircraft around the airfield when it is taking–off or landing). The longitudinal axis of the airplane is centered with the centerline of the runway. After this alignment, a final flap settings is completed and pitch attitude is adjusted for desired angle of descent. The speed of an airplane in this phase should be about 1.3 times the stall speed. A stabilized descent angle is maintained

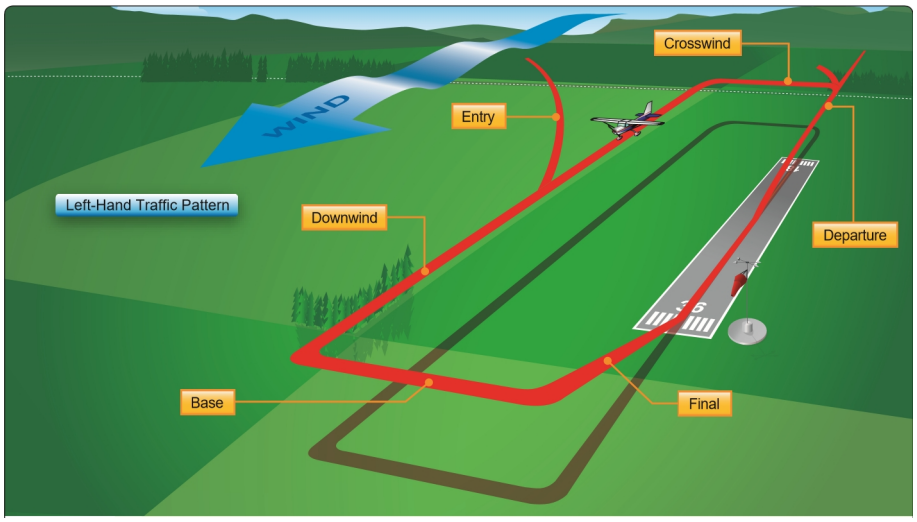

Figure 2.6: Airfield traffic pattern (left–hand). Note positions of the base and the final [8].

throughout this phase so as to land the airplane on the centerline in the first third of the runway. The objective is to descend at an angle and airspeed that permits the plane to reach the touchdown point at the airspeed that requires minimum floating before touchdown, a semi–stalled condition in essence [8].

The round out (flare)

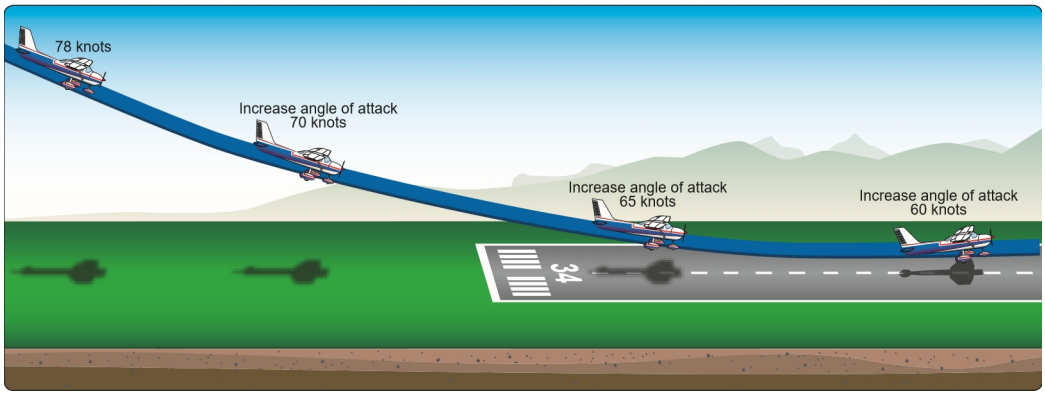

Figure 2.7: The round out[8].

The round out is a slow, smooth transition from the normal approach attitude to the landing attitude (figure 2.7). In other words, it is rounding the flightpath with the one that is parallel with runway and within few centimetres above it. The round out typically starts at 3 to 6 metres above the ground and is a continuous process until the airplane touches down. The rate of the round out depends on the airplane's height above the ground, descent rate and pitch attitude. If the round out is started too high above the ground, it must be performed more slowly than the round out started at the lower height to allow the airplane to descend to the ground while the proper landing attitude is being established. It must be also proportionate to the rate of closure with the ground [8].

Visual cues are usually used when performing flare in proper altitude and maintaining airplane's wheels a few decimeters (0.5 - 1 m [15]) above the ground before the touchdown. These cues are primarily dependant on the angle at which pilot's central vision intersects the runway ahead and slightly to the side. A proper depth reception is necessary, but the cues used most are those related to the change of the size of familiar objects in the landing area such as airport buildings, fences or trees. Recommended technique is to focus direct central vision at downward angle 10 to 15 degrees towards the runway as the round out is initiated. Forward or backward movement of the visual interception point then indicates loss or gain of the altitude [8].

The touchdown

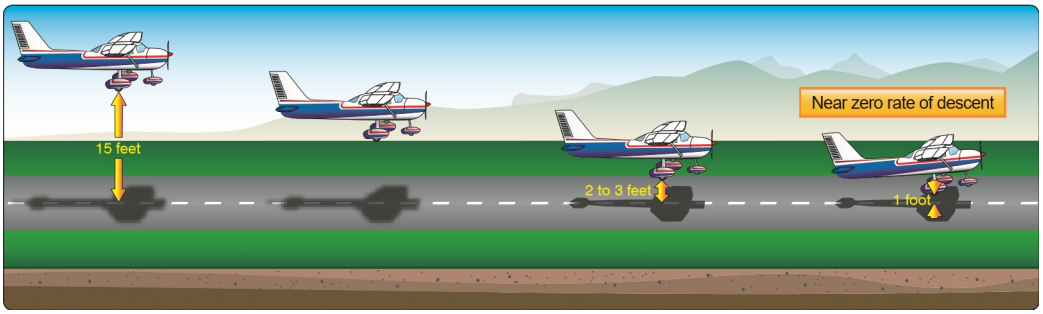

Figure 2.8: The round out and touchdown [8].

The touchdown (see the figure 2.8) is a gentle settling of the airplane onto the runway. The round out and the touchdown are usually made with the power set at idle and the airplane at minimum controllable speed so that the airplane touches down on main gear at approximately stalling speed and at minimal vertical speed. Should these conditions are not met, for example due to the inaccurate estimate of the height above the ground, the airplane may crash land because of stalling too high above the runway, touching down at too high vertical speed or may bounce back to the air and possibly overrun the runway (or perform the go–around if possible) [8].

Summary

This chapter provided the brief description of the modern height–measuring devices in aviation, as well as the description of the final phase of the flight, the landing. Its aim was to familiarize the reader with this topic and provide the necessary information related to the thesis.

Chapter 3

Radar and radar signal processing

A radar is an electromagnetic device which serves the purpose of detection, location, tracking and recognition of reflecting objects of various kinds, sometimes at considerable distance [21]. The radar itself is an electronic device, but with strong relations to the information technology field. This thesis deals with the digital signal processing of the radar signal, which is one example of such relation. The others may be the control software in radar modules or displaying the information gained from the radar signal in human–comprehensible form where the techniques and knowledge from the computer graphics are used.

The aim of this chapter is to provide the significant or thesis–related facts about the radar systems and subsequent radar signal processing and therefore can not be considered encyclopaedic overview of the whole radar field.

3.1 Early radar development

The idea of radar emerged in the late 1880s, when German physicist Heinrich Hertz decided to experimentally verify theoretical work of Scottish physicist James Clerk Maxwell who formulated general equations of the electromagnetic field, determining that both light and radio waves are examples of electromagnetic waves governed by the same laws, but having significantly different frequencies. This led to the conclusion that radio waves as such can be reflected by metallic objects and refracted by dielectric objects in the same way as the light can. Hertz carried out an experiment which demonstrated these properties using radio waves at a wavelength of 66 cm (which corresponds to the frequency 455 MHz) [21].

In 1904, a patent for obstacle detector and ship navigation device based on Hertz's work was issued to German engineer Christian Hülsmeyer, however, as there was no need for such device at the time, it wasn't until 1930s that a serious radar development commenced, mainly prompted by the progress in military aviation and availability of long–range bombers. Many countries suddenly began to look for a means with which to detect approaching enemy aircraft. Probably the most famous of these efforts was the British early–warning radar system called Chain Home [21].

3.2 Principle of operation

The principle of operation of the radar can be summarized into the following steps [20], illustration is shown in the figure 3.1:

- The radar radiates electromagnetic energy from the antenna.

- The radiated energy propagates in the space.
- Some of the energy is intercepted by a reflecting object (usually called the *target*), located at a distance from the radar.
- The energy intercepted by the target is reradiated in many directions.
- Some of the reradiated energy (called the *echo*) is returned and received by the radar antenna.
- The receiver amplifies received signal and makes a decision whether or not a target echo is present. Target location and possibly other information about the target is acquired.

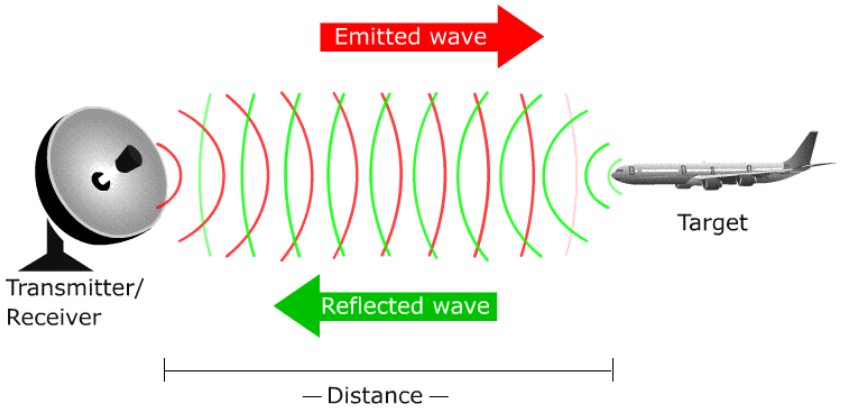

Figure 3.1: The principle of radar operation [19].

3.3 Doppler Effect

The Doppler effect is the change of the frequency or pitch when a transmitter and the target move relative to the each other. The Doppler effect, named after the Austrian physicist Christian Doppler, is not reserved only to radar waves, but applies to all wave motion including sound waves. Therefore, probably everyone has experienced the Doppler effect even without realisation. The most common example is the sound of the siren of passsing emergency vehicle [23].

Frequency change

If the frequency of a signal (let's assume sound signal) from the transmitter is constant, the wavelength of the sound will also remain constant. If both the transmitter and receiver remain stationary, the receiver will hear the same frequency as the transmitter produces. That is because the receiver receives the same number of waves per second as the transmitter produces [23].

If the transmitter and the receiver travel towards each other (it does not matter which one is actually moving or whether both of them are moving), the receiver will perceive a higher frequency sound. That is because the receiver will receive a higher number of

sound waves per second than the transmitter produces and will interpret this as a sound of the higher frequency. Each wave has a shorter and shorter distance to travel to reach the receiver and therefore the waves arrive with decreasing intervals between them. Vice versa, if the transmitter and receiver are moving from each other, the receiver will receive a lesser number of waves per second and will interpret this as a lower frequency sound [23]. The illustration of the Doppler effect is shown in the figure 3.2.

Figure 3.2: The Doppler effect; the car is moving to the left [23].

The equation of Doppler frequency is given as follows [23]:

$$f_D = \frac{2v_r}{\lambda} = \frac{2v_r f_{tx}}{c_0} \tag{3.1}$$

where f_D $[Hz]$ is Doppler frequency, v_r $[m.s^{-1}]$ is the speed of the motion between the transmitter and the receiver (radial speed, $\lambda\,[m]$ is the wavelength, f_{tx} is the transmitter signal frequency and c_0 is the speed of light. Please note that the speed of the motion is multiplied by 2, because the wave has to travel from the radar antenna to the target and back.

3.4 Frequency–Modulated Continuous–Wave Radar

Frequency–Modulated Continuous–Wave radar (FMCW radar) is a special type of the radar, which radiates a continuous transmission power much like a Continuous–wave radar (CW radar), but in contrast to the CW radar, it changes its operational frequency during measurement by modulating the transmission signal (common modulation patterns are shown in the figure 3.3) in frequency (or in phase) [24].

Basic continuous–wave radars without frequency modulation suffer from disadvantage of not being able to determine the range to the stationary target because they lack the timing marks, which would allow the system to accurately time the transmitting and receiving cycle and convert it into a range. These marks can be generated using frequency modulation, which means that the transmitted signal frequency periodically increases and decreases. When an echo signal is received, that change of frequency gets a delay δ_t according to the difference in the frequency or in the phase between the transmitted and the received signal (figure 3.4) [24].

The FMCW radar usually consists of two main parts: a transceiver and a control unit with the microprocessor. The block diagram of the FMCW radar is shown in the figure 3.5. Green color denotes parts of the control unit and yellow color denotes parts of the transceiver. Arrows show the direction of the signal propagation. The input is the control word which is converted to analoguos control voltage by the digital–to–analog converter. According to this voltage, the Voltage Controlled Oscillator changes its frequency. The signal is subsequently filtered by the band filter, which blocks spikes and harmonics. The coupler branches off part of the transmission power to the receiver (reference

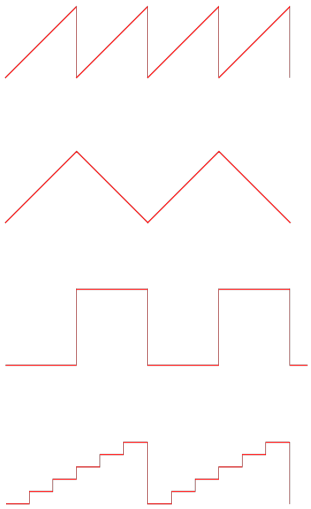

Figure 3.3: Common modulation patterns. Top to bottom: sawtooth, triangular, rectangular and staircase voltage [24].

frequency). Transmission power then may be amplified and is send to the transmitting antenna. The receiver antenna converts the oncoming signal back into the RF voltage. The echo signal is usually weak and is therefore amplified by the low–noise amplifier. The mixer compares echo signal with current transmission frequency and outputs the difference between them which then passes through the low–pass filter and another amplifier to the analog–to–digital converter [24].

FMCW radar features and usage

Frequency–modulated continuous–wave radars have several distinctive features [16]:

- Ability to measure small and very small ranges to the target, minimal range is comparable to the transmitted wavelength.
- Ability to measure simultaneously the target range and its relative speed.
- Small error of measurement, which with some processing methods is hundredths or even thousandths of a percent.
- Ability to measure small changes of a range (less than a fraction of a wavelength).
- Ability to use various types of indicators.
- Signal processing after mixing is performed in a range of frequencies commensurable with the modulation frequency, considerably simplifying the processing circuits.
- Safety from the absence of pulse radiation.
- Compactness, the dimensions of a radar using modern technology being determined by dimensions of a microwave block
- Small weight and energy consumption due to the absence of high circuit voltages.

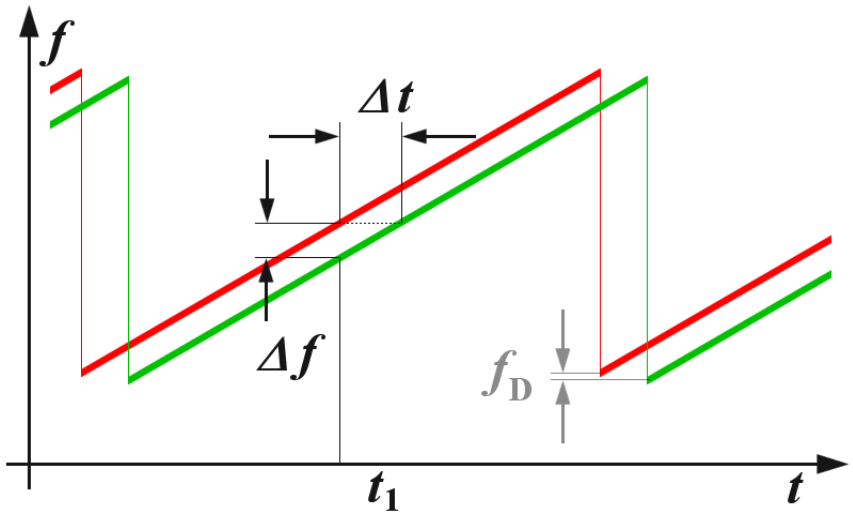

Figure 3.4: Ranging using the FMCW radar [24].

- Possible application of ultrasonic transmissions.

Examples of applications of the FMCW radar include: a radio altimeter, level–measuring radar in water tank, navigational radar, vehicle collision warning systems, precision range meter for fixed targets and measurement of very small motions [16].

FMCW radar general signal expressions

The expression for the transmission of the FMCW radar is as follows [16]:

$$u_p(t) = U_p(t)\cos\phi_p(t) \tag{3.2}$$

where $U_d(t)$ is the amplitude of the signal and $\phi_d(t)$ is its phase. A sample of FM signal passes to the mixer. This signal, called the direct signal, can be expressed as:

$$u_d(t) = U_d(t)\cos\phi_d(t) \tag{3.3}$$

The reflected signal of a stationary object is delayed by the propagation time:

$$\tau = \frac{2R}{c} \tag{3.4}$$

where R is the range (distance) to the reflecting object, which is multiplied by 2, because the signal has to travel to the object and back to the transceiver and c is the speed of light, or, to be more precise, the speed of the propagation of electromagnetic waves in the given environment [22]. If the object with initial range R_0 (at $t_0 = 0$) moves with some radial velocity v, the delay will not be constant. Under the condition $v \ll c$, it will be almost linear function [22]:

$$\tau \approx \frac{2}{c}(R_0 + vt) \tag{3.5}$$

where t is the time. It is usually assumed that the reflected signal is a copy of the transmitted signal delayed by the propagation time and can thus be written as:

$$u_r = U_r(t,\tau)\cos\phi_r(t,\tau) = k_1\, U_r(t-\tau)\cos\left[\phi_p(t-\tau) + \phi_0\right] \tag{3.6}$$

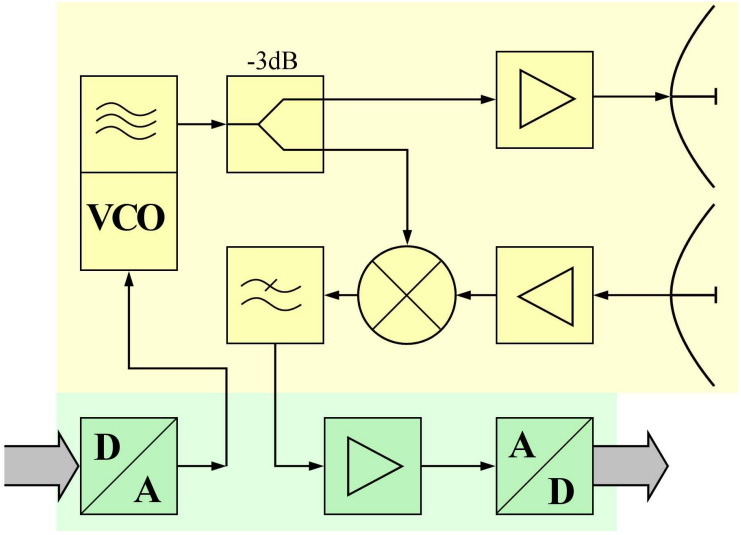

Figure 3.5: A block diagram of the FMCW radar [24].

where k_1 expresses the reduction in its amplitude and ϕ_0 is the phase shift caused by the reflecting properties of the target. As the reflecting signal entering the mixer is much less than the direct signal, the mixer output can be written as [16]:

$$u_t(t) = k_2 U_r(t,\tau) \cos\left[\phi_d(t) - \phi_r(t,\tau) - \phi_0\right] + k_3 U_d(t) \tag{3.7}$$

where k_2 and k_3 are factors describing mixer voltage gains in conversion and amplitude detection gains.

The mixer output will be called converted signal. It may be also called intermediate frequency. Only the first term is useful, containing the information on target range and the speed relative to the FM radar. The second term is parasitic signal and has no influence on useful signal [16].

FMCW radar signal processing using 2D DFT

For the processing, let's assume a signal shown in figure 3.6 which shows both the transmitted (continuous line) and received signal (dashed line). The signal is modulated with low–frequency waveform of sawtooth shape and period T.

The received signal is mixed with the attenuated transmitted signal and after low–pass filtering a low (differential) frequency signal called the converted signal is obtained. This converted signal is approximately sinusoidal with frequency f_w, which is constant in the time interval $T - \tau$ and which equals the change of the transmitter frequency during time τ [22].

$$f_w = \alpha\tau \tag{3.8}$$

where α is the modulation waveform slope:

$$\alpha = \frac{\Delta f}{T} \tag{3.9}$$

where Δf is the maximum frequency deviation:

$$\Delta f = f_{max} - f_{min} \tag{3.10}$$

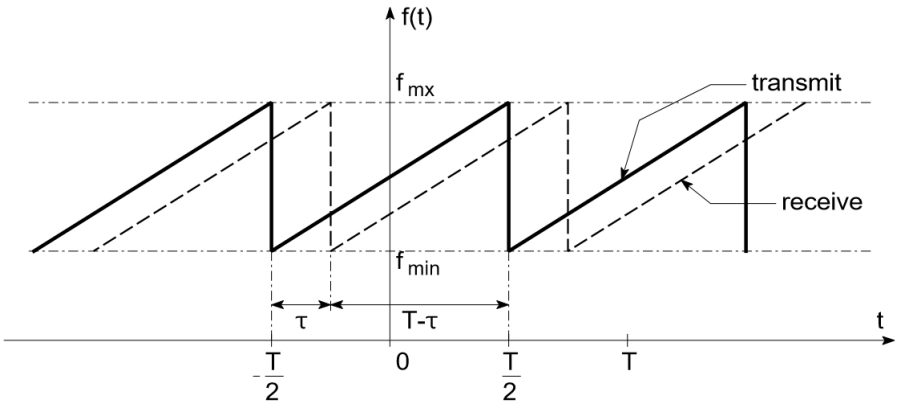

Figure 3.6: A sawtooth signal. The frequency of transmitted and received signal [22].

The measurement of a stationary object range R is equivalent to determining the frequency of the converted signal during the $T - \tau$ interval [20].

$$R = \left| T \frac{c\Delta f}{2f} \right| \tag{3.11}$$

If the target object has radial velocity, the time delay is not constant (the expression 3.5). As the delay change is relatively slow, it can be noticed only in the phase change of the converted signal. If the signal is analyzed in K modulation periods, the Doppler frequency can be estimated from the phase change and subsequently the target velocity can be computed [22].

The FMCW radar emits the signal:

$$u(t) = U\cos(\phi(t)), -\infty < t < \infty \tag{3.12}$$

where the frequency is a periodical function of time shown in figure 3.6:

$$f(t) = \frac{1}{2\pi}\frac{d\phi(t)}{dt} = f_{min} + \alpha(t - kT),\ kT - \frac{T}{2} < t < kT + \frac{T}{2},\ (k = 0, \pm 1, \ldots) \tag{3.13}$$

The received signal is [22]:

$$u_0(t) = U_0\cos(\phi_0(t)), -\infty < t < \infty \tag{3.14}$$

and is delayed by the propagation time τ. Upon mixing with attenuated copy of $u(t)$ and low–pass filtering, a converted signal is obtained [22]:

$$x(t) = \cos(\phi_w(t)), -\infty < t < \infty \tag{3.15}$$

The converted signal differential phase can be described by the equation [22]:

$$\phi_w(t_k) = \begin{cases} 2\pi f_0\tau - \pi\alpha[(T-\tau)^2 + 2(T-\tau)t_k] & -\frac{T}{2} < t_k < -\frac{T}{2} + \tau \\ 2\pi f_0\tau - \pi\alpha[(\tau^2 - 2\tau t_k] & -\frac{T}{2} + \tau < t_k < -\frac{T}{2} \end{cases} \tag{3.16}$$

where t_k is:

$$t_k = t - kT, k = 0, \pm 1, \ldots \tag{3.17}$$

When the instrumental range of the radar equals R_{max}, the signal reflected from the target object at this distance equals τ_{max}, therefore the effective time of video signal observation in one modulation cycle equals $T - \tau_{max}$ [22].

After the substition of the equation 3.5 into the equation 3.16 and deleting unimportant quadratic components, we get [22]:

$$\phi_w t_k \approx 2\pi\big[f_0\tau_0 + kf_dT + (f_w + f_d)t_k\big], -T/2 + \tau < t_k < T/2 \tag{3.18}$$

where:

$$f_d = \frac{2v}{c} f_0 \tag{3.19}$$

is the Doppler frequency and f_w is the converted signal frequency corresponding to the stationary object at range R_0:

$$f_w = \alpha\tau_0 \tag{3.20}$$

The equation 3.18 shows that the range measurement is disturbed with an error dependent on the target object velocity as the frequency f_d shifts the value of frequency f_w. This error can be corrected after determining the object velocity [22].

The range information itself is contained in the Fourier spectrum of the converted signal $x(t)$ [22]:

$$X_r(\omega, k) = \int_{-T/2+\tau_{max}}^{T/2} x(t_k) e^{-j\omega t_k} dt_k \tag{3.21}$$

computed for one modulation period (k). The absolute value of the Fourier spectrum $|X_r(\omega, k|$ attains the maximum for the angular frequency [22]:

$$\omega = \pm 2\pi(f_w + f_d) \tag{3.22}$$

The spectrum is a function of k as the angle $2\pi k f_d T$ changes with k. The information about the movement of the object (the velocity) is contained in this change. If the function $X_r(\omega, k)$ is treated as the discrete function of k with sampling period T, its spectrum $X(w, \theta)$ observed in K consecutive modulation periods is [22]:

$$X(w, \theta) = \sum_{k=0}^{K-1} X_r(\omega, k) e^{-jk\theta} \tag{3.23}$$

where:

$$\theta = w_v T \tag{3.24}$$

where w_v is the velocity frequency. To determine the object velocity, it is necessary to compute the spectrum 3.23 and find the frequency θ_d where the absolute value of the spectrum attains its maximum. This frequency is equal to [22]:

$$\theta_d = 2\pi f_d T \tag{3.25}$$

where f_d is the Doppler frequency. The spectrum is a periodic function θ. thus the measurement of f_d is ambiguous outside the range $-\frac{1}{2T} < f_d < \frac{1}{2T}$. The maximum unambiguously measured velocity is [22]:

$$v_{max} = \frac{c}{4Tf_0} \tag{3.26}$$

Two dimensional spectrum is usually computed with digital methods. Firstly, the range spectrum of signal $x(t)$ sampled with frequency f_p is computed with N-point discrete Fourier

transform for every modulation period using the fast Fourier transform method. Then the spectrum 3.23 is computed using K-point DFT [22]. Of course, when the information about the object velocity is not required or it is certain that the effect of Doppler frequency is negligible for our purposes, this part of the computation may be omitted.

Note about triangular modulation

The text above considered the sawtooth modulation. However, the sawtooth modulation is very similar to the triangular modulation (shown in the figure 3.7), which has interesting advantage when it comes to the radar signal processing [24].

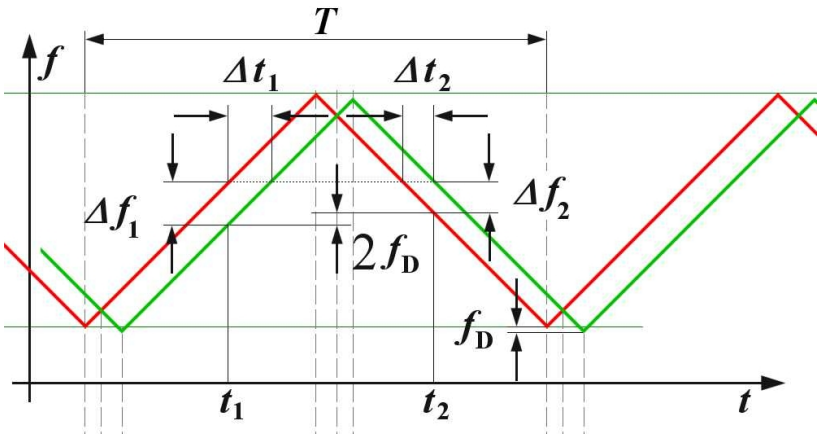

Figure 3.7: The triangular modulation [24]

This modulation pattern has, on the contrary to the sawtooth modulation, two edges (slopes) of modulation. Therefore, the distance measurement can be performed on both of these edges. In the figure 3.7, the received signal is shifted in x–axis due to the time delay and in the y–axis due to the Doppler frequency [24].

The measured frequency is then the sum of the range frequency and Doppler frequency at the rising edge of the modulation cycle and the difference of them at the falling edge.

The Doppler frequency then can be determined as an arithmetic average of the two measurements at different edges of the modulation pattern. The difference between the two difference frequencies is twice the Doppler frequency. The measured frequency (denoted $f_{/\sum}$) is shown in the figure 3.8). The formulas are [24]:

$$f(R) = \frac{\Delta f_1 + \Delta f_2}{2} \tag{3.27}$$

for the frequency used for range computation (hence the „R“). And the following formula for the Doppler frequency:

$$f_D = \frac{|\Delta f_1 - \Delta f_2|}{2} \tag{3.28}$$

where the δf_1 and δf_2 are frequency differences at the rising and the falling edge, respectively [24].

The ability to correct the measured range using the Doppler frequency is an advantage over the sawtooth modulation, where the Doppler frequency for one modulation cycle cannot be determined and the algorithm either has to do without this information (which may or

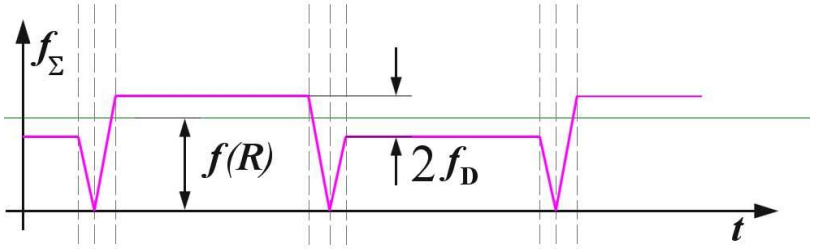

Figure 3.8: Range $f(R)$ and Doppler f_D frequencies for the triangular modulation [24].

may not be a problem) or a computation of 2D DFT over several modulation cycles has to be used.

Comparison of sawtooth and triangular modulation

As such, it can be said that the triangular modulation is the most useful or convenient type of the modulation provided that the particular application requires the knowledge of the Doppler frequency (because of the expected movement of the target). The sawtooth modulation may be used if no significant movement is suspected or the correct information about the target range while moving is not needed. Because many commercially available radar modules support different types of the modulation, the modulation pattern can be easily chosen to fit the particular application and its requirements.

Chapter 4

Digital signal processing basics

As the signal that radar receives is of course analog, whilst the processing is (at least in our case) digital, this chapter provides basics about digital signal processing in general. The following overview is, rather than a complete list, a selection of techniques used either in the implementation part of the thesis itself or in the radar signal processing as such. If not stated otherwise, the following text and figures have been adapted from [13].

4.1 Signal processing scheme

The whole digital signal processing can be summarized into the following scheme:

$$\xrightarrow{\text{x(t)}} A/D \xrightarrow{\text{x[n]}} \text{Processing} \xrightarrow{\text{y[n]}} D/A \xrightarrow{\text{y(t)}}$$

where $x(t)$ is the input (analog) signal with continuous time defined (in the time domain) from $-\infty$ to ∞, which is transformed by the Analog–to–digital converter into the $x[n]$ discrete (sampled) signal. Subsequent digital processing creates discrete $y[n]$ output signal. This signal can be then converted back to the analog form using Digital–to–analog converter if such conversion is needed for the particular application. However, lot of applications do not require such conversion as they then process digital information gained from signal or store it.

The processing is often done by transforming the signal from the time domain to the frequency domain using the Fourier Transform:

$$X(f) = \int_{-\infty}^{+\infty} x(t) e^{2\pi f t} dt \tag{4.1}$$

where $X(f)$ is called spectral function, which is complex and defined for each f from $-\infty$ to ∞. The f is the frequency, t stands for the time and $x(t)$ is the original analog signal. This function has modulus $|X(f)|$ and argument $\angle X(f)$. For real signals, right ($f > 0$) and left parts of the spectral functions are complexly conjugated:

$$X(f) = X * (-f) \tag{4.2}$$

For the modulus and the argument:

$$|X(f)| = |X(-f)| \tag{4.3}$$

$$\arg X(f) = -arg|X(-f)| \tag{4.4}$$

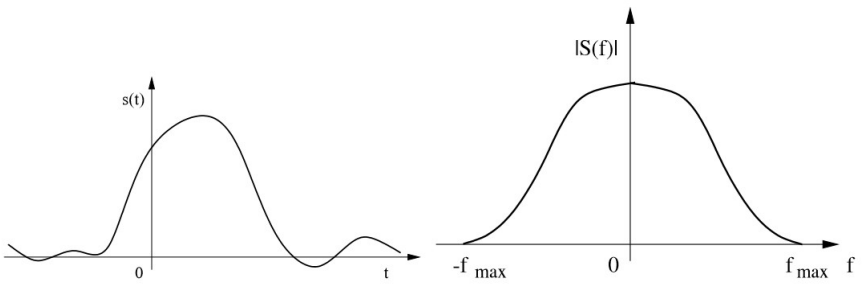

Figure 4.1: The analog signal and its spectral function

4.2 Analog–to–digital conversion

The first stage of digital signal processing is the Analog–to–digital converter. As mentioned before, it transforms the analog input signal with continuous time to the sampled signal with discrete time. This process could be illustrated as a three–stage process:

$$\xrightarrow{x(t)} \text{AAF} \rightarrow \text{Sampling} \xrightarrow{xs[n]} \text{Quantization} \xrightarrow{xq[n]}$$

where „AAF“ stands for the anti–aliasing filter.

Sampling

A sampled signal is gained by multiplying the original (analog, continuous–time) signal by the sequence of periodical rectangle impulses.

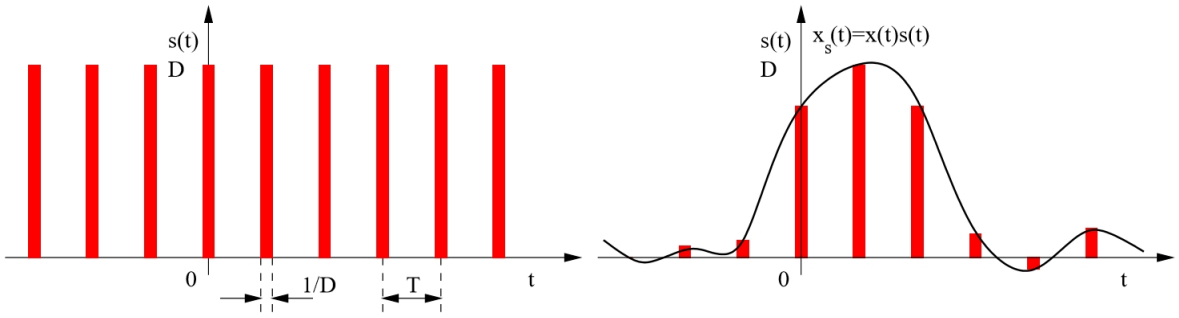

Figure 4.2: Multiplying the analog signal by the sequence of rectangular impulses

In theory, the multiplying is done by multiplying the signal by the sequence of Dirac impulses (the unit impulse), which is infinitely high, has zero width and its integral has the value of 1. Dirac impulses in this sequence are spaced by T (the sampling period), whilst the $F_s = 1/T$ is the sampling frequency.

This sequence of Dirac impulses is also called Dirac comb, impulse train or sampling function. After the multiplication, a similar series of Dirac impulses is gained, this time, however, with integral equal to the values of the sampled signal at the nT points.

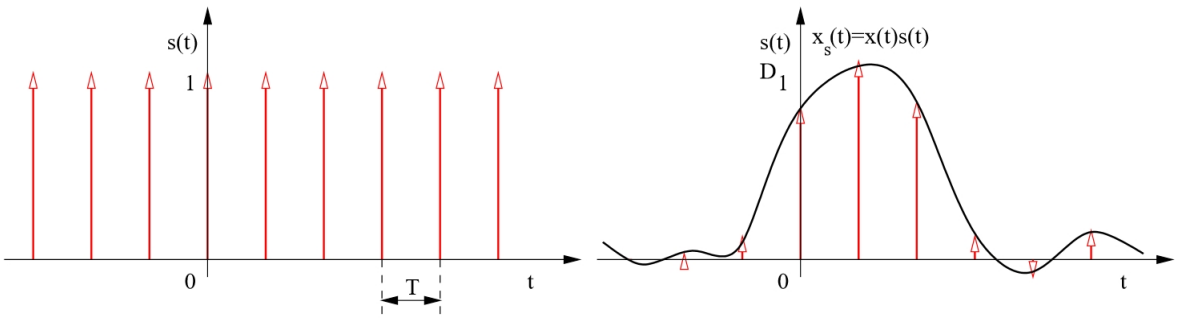

Figure 4.3: Multiplying the analog signal by the sequence of Dirac impulses (Dirac Comb)

The spectrum of the sampled signal is periodic:

$$X_s(f) = \frac{1}{T}\sum_{n=-\infty}^{\infty} X\left(f - \frac{n}{T}\right) = \frac{1}{T}\sum_{n=-\infty}^{\infty} X\left(f - nF_s\right) \tag{4.5}$$

Supposing there is a maximum frequency in the signal f_{max} a two situations may happen:

1. $F_s > 2F_{max}$ Copies of the original spectrum *do not overlap* and it is possible to ideally reconstruct the original signal using the low–pass filter with cutoff frequency $F_s/2$. This situation is shown in the figure 4.4.

2. $F_s < 2F_{max}$ Copies of the original spectrum *do overlap* and the resulting spectrum has a different shape than the original one. It is not possible to reconstruct the original signal due to the aliasing effect. This situation is shown in the figure 4.5

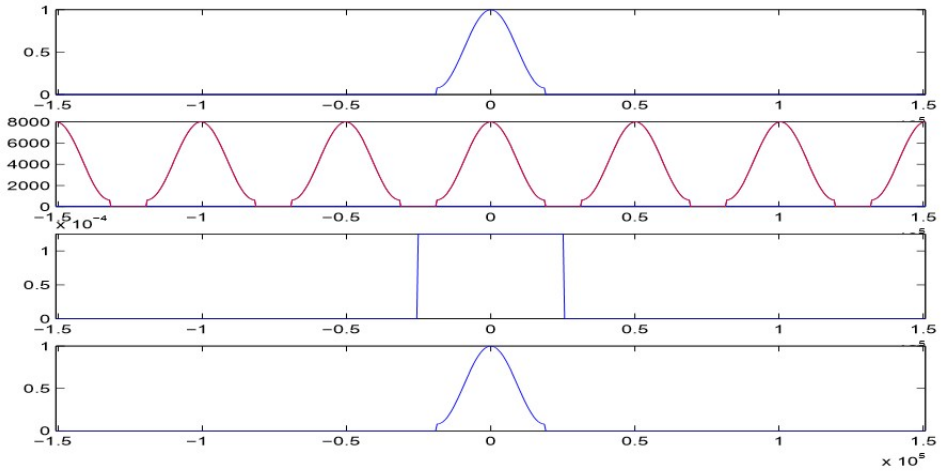

Figure 4.4: From Top to Bottom: the original spectral function, the spectral function of the sampled signal, the reconstruction low–pass filter and the spectral function of the reconstructed signal

The sampling theorem (also called Shannon theorem, Nyquist–Shannon theorem, Kotelnikov theorem or even Nyquist–Shannon–Kotelnikov theorem) then states the following

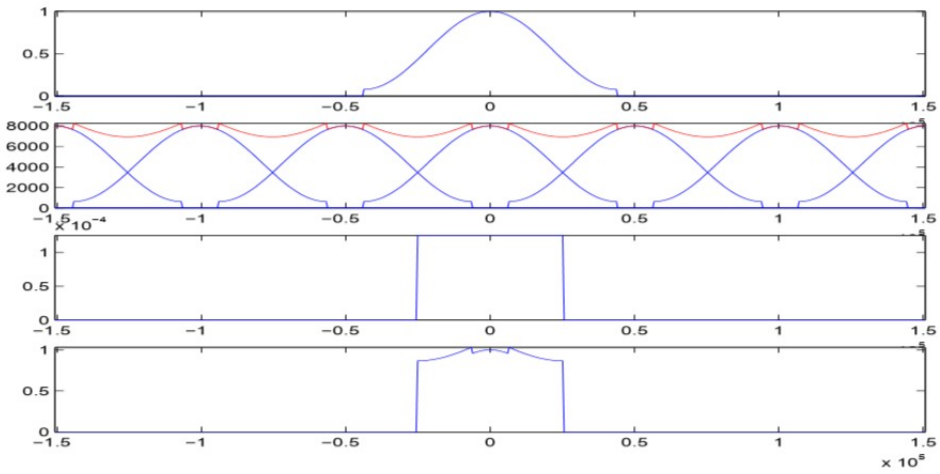

Figure 4.5: From Top to Bottom: the original spectral function, the spectral function of the sampled signal, the reconstruction low–pass filter and the spectral function of the reconstructed signal (in this case different than the original one)

condition for the ideal sampling which, if it is met, prevents the aliasing effect:

$$F_s > 2f_{max} \tag{4.6}$$

To better illustrate the aliasing problem, following figures show a cosine signal sampled with such sampling frequency that the sampling theorem condition is not met. The figure 4.6 shows the original signal and sampling, while the figure 4.7 shows the reconstructed signal. Both figures are in the time domain.

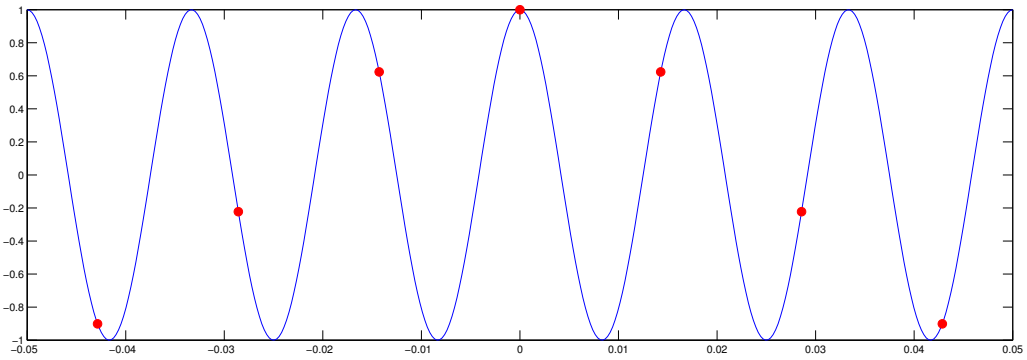

Figure 4.6: A cosine signal with $f_{max} = 60\,Hz$; $F_s = 70\,Hz$. Red points shows the sampling points.

Anti–aliasing filter

The anti–aliasing filter is used so that the condition stated by the sampling theorem is met, albeit „artificially“. This filter limits the frequency range of the original signal to

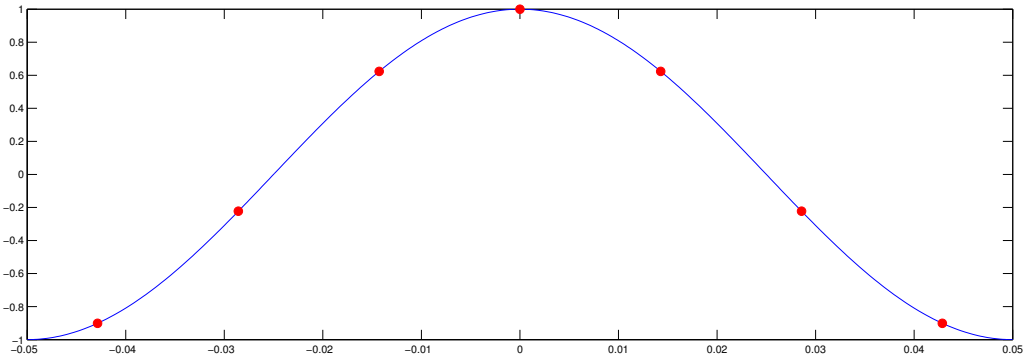

Figure 4.7: The reconstructed signal from sampling of the signal from figure 4.6. Red points represent the original sampling points.

$[-F_s/2, F_s/2]$. Even though some frequencies are „lost“, the damage caused by the anti–aliasing filter is somewhat smaller than the damage caused by the aliasing effect. The difference of results is shown in the figure 4.8 (see the figure 4.5 for the comparison)

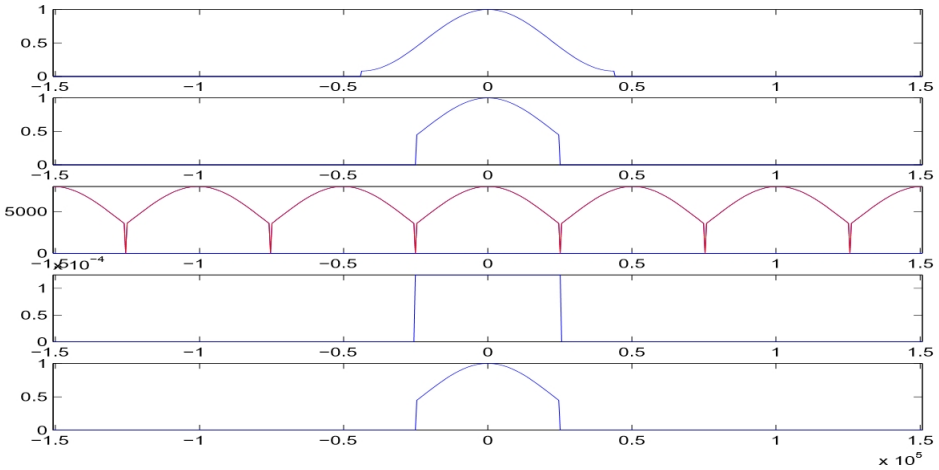

Figure 4.8: From Top to Bottom: the original spectral function, the spectral function after being processed by the anti–aliasing filter, the spectral function of the sampled signal, the reconstruction low–pass filter and the spectral function of the reconstructed signal.

Quantization

After the sampling, a quantization stage takes place. The sampled signal is quantized, in other words, the input values of the original signals are mapped onto the smaller set of values, called quantization levels. This mapping can be expressed as [17]:

$$xq[n] = Q_N(xs[n]) \tag{4.7}$$

where Q_N is the mapping function.

Generally speaking, m quantization levels are used. To express m quantization levels, N bits are needed:

$$N = \log_2 m \tag{4.8}$$

The signal–to–noise ratio (SNR) is equal to:

$$SNR = 6N + K \tag{4.9}$$

where K is constant dependent on the character of the signal.

During the process of quantization, as the quantization mapping function maps a certain range of the input values to the one specific value (quantization level), errors occur due to the rounding–off or truncation, as the mapping function maps the real values to the integer ones [17]:

$$xs[n] \in \mathbb{R} \xrightarrow{Q_N} xq[n]\mathbb{Z} \tag{4.10}$$

This error is commonly referred to as quantization error or quantization noise. For better illustration of quantization process, an example of the original signal andthe quantized one is provided in the figure 4.9.

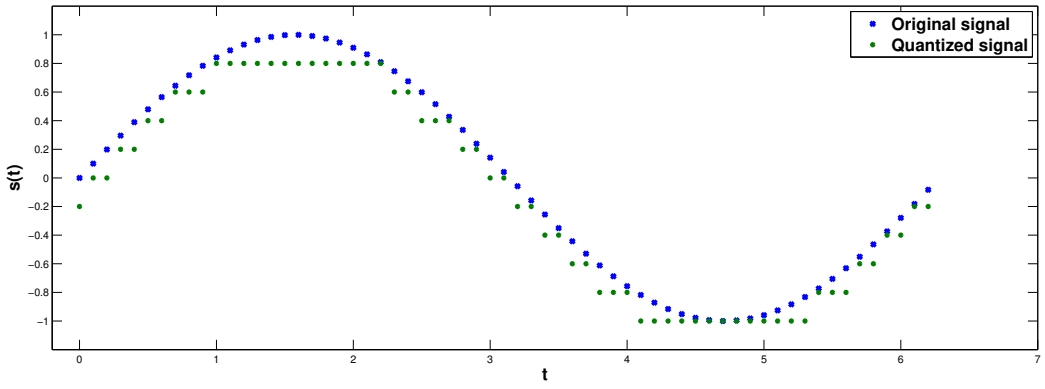

Figure 4.9: A quantization of the signal [3]

4.3 Linear filtration

Linear filters are used to change the frequency characteristics of the signal. The simple scheme of the usage of the linear filter is:

$$\xrightarrow{\text{x[n]}} \text{Linear Filter} \xrightarrow{\text{y[n]}}$$

The usual characteristics of the linear filters are:

- *the linearity*: linear filters maintain linear combination. If $x_1[n] \to y_1[n]$ and $x_2[n] \to y_2[n]$, then $ax_1[n] + bx_2[n] \to ay_1[n] + by_2[n]$, where $a, b \in \mathbb{R}$
- *the time invariance*: linear filters do not change their behaviour over time; if $x[n] \to y[n]$, then $x[n - n_0] \to y[n - n_0]$, where n_0 is the arbitrary time shift.
- *the causality*: . The output $y[n]$ is only dependent on the past samples (the linear filter does not see „the future“): $y[m < n]$ and $x[m < n]$

Linear filter impulse response

The impulse response of linear filters is the response of the filter should the filter receive the Kronecker delta as the input:

$$\delta[n] = \begin{cases} 0 & \text{for } n \neq 0 \\ 1 & \text{for } n = 1 \end{cases} \tag{4.11}$$

Let the impulse response be $h[n]$, then the filter scheme is:

$$\xrightarrow{\delta[n]} \text{Linear Filter} \xrightarrow{\text{h[n]}}$$

Knowing the impulse response of the linear filter, it is possible to compute the response of the filter for any input signal as each input sample causes one impulse response, multiplied by the value of the input sample. These impulse responses add together because the filter is linear. This can be written as a convolution:

$$y[n] = x[n] * h[n] = \sum_{m=-\infty}^{\infty} x(m)h(n-m) = \sum_{m=-\infty}^{\infty} h(m)x(n-m) \tag{4.12}$$

The impulse response may have the following features:

- if $h(k) < 0$ for $\forall k < 0$ then the filter is casual, as all samples after the $n-th$ will not be multiplied by anything other than zero.
- the impulse response may be finite (FIR filter - finite impulse response) or infinite (IIR - infinite impulse response)
- the Fourier transform in the frequency domain shows the complex frequency characteristics of the filter: $h(k) \rightarrow H(f)$

The spectrum of the resulting signal is as follows because the convolution in the time domain represent multiplication in the frequency domain:

$$Y(f) = X(f)H(f) \tag{4.13}$$

Filter difference equation

The behaviour of the linear filter can be described by the difference equation:

$$y[n] = \sum_{k=0}^{Q} b_k x(n-k) - \sum_{k=1}^{P} a_k y(n-k) \tag{4.14}$$

where $x(n-k)$ are current and delayed samples of the input and $y(n-k)$ are delayed samples of the output. According to the this equation, the general scheme of the linear digital filter looks as shown in the figure 4.10 According to the values of coefficients b_k and a_k, it is possible to distinguish between three types of digital linear filters:

1. **FIR filter** - a finite impulse response filter. Only the $b_0 \dots b_Q$ coefficients are non–zero. This type of filter is always stable.
2. **pure IIR filter** - an infinite impulse response filter. Only the coefficients b_0 and $a_0 \dots a_P$ are non–zero.
3. **general IIR filter** - infinite impulse response filter. Coefficients a_i and b_i are non–zero.

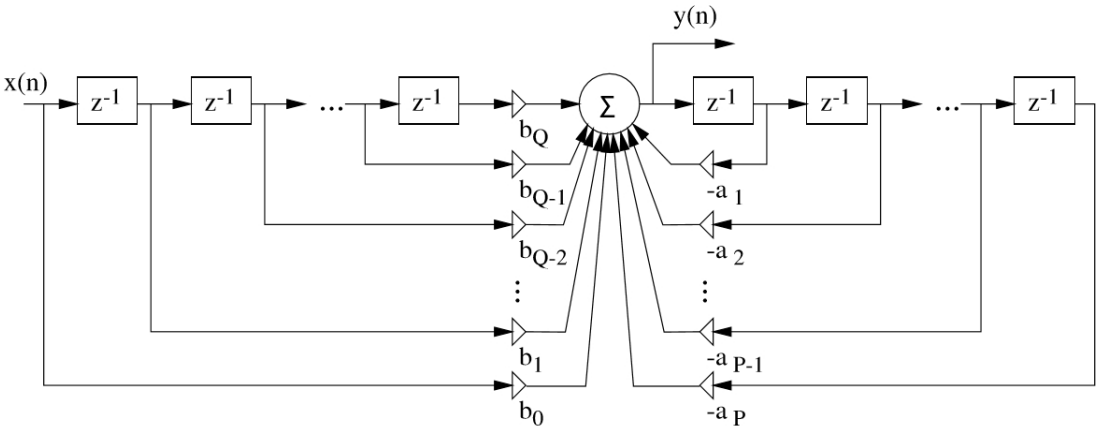

Figure 4.10: A general scheme of the digital liner filter. Block z^{-1} denotes the unit delay [13]

4.4 Signal processing

After the original analog (continuous–time) signal is converted to the digital (discrete–time) signal, the actual processing may take place. The processing itself may be of many different kinds, depending on the particular application. It may be required only want to store the signal, alter the signal in any way or gain some information about it. This third option is the case of this Master's thesis and therefore will be described.

Of course, sometimes after the processing stage, the signal needs to be converted back again to the analog form in order to show the results in the form comprehensible for humans. This is done by digital–to–analog converters, but, as this is not needed for our purposes, it will not be described.

Preprocessing

The DC offset of the signal carries no useful information and can even interfere during processing (the energy computation). Therefore it is advisable to remove it by subtracting the mean value of the signal:

$$s'[n] = s[n] - \mu_s \tag{4.15}$$

where μ_s is the mean value of the signal, which needs to be computed or estimated. There are two basic ways how to obtain the mean value of the signal:

Offline computation of mean value

The offline mean value of the signal is computed as a simple average value of samples:

$$\bar{s} = \frac{1}{N} \sum_{n=1}^{N} s[n] \tag{4.16}$$

The result is shown in the figure 4.11.

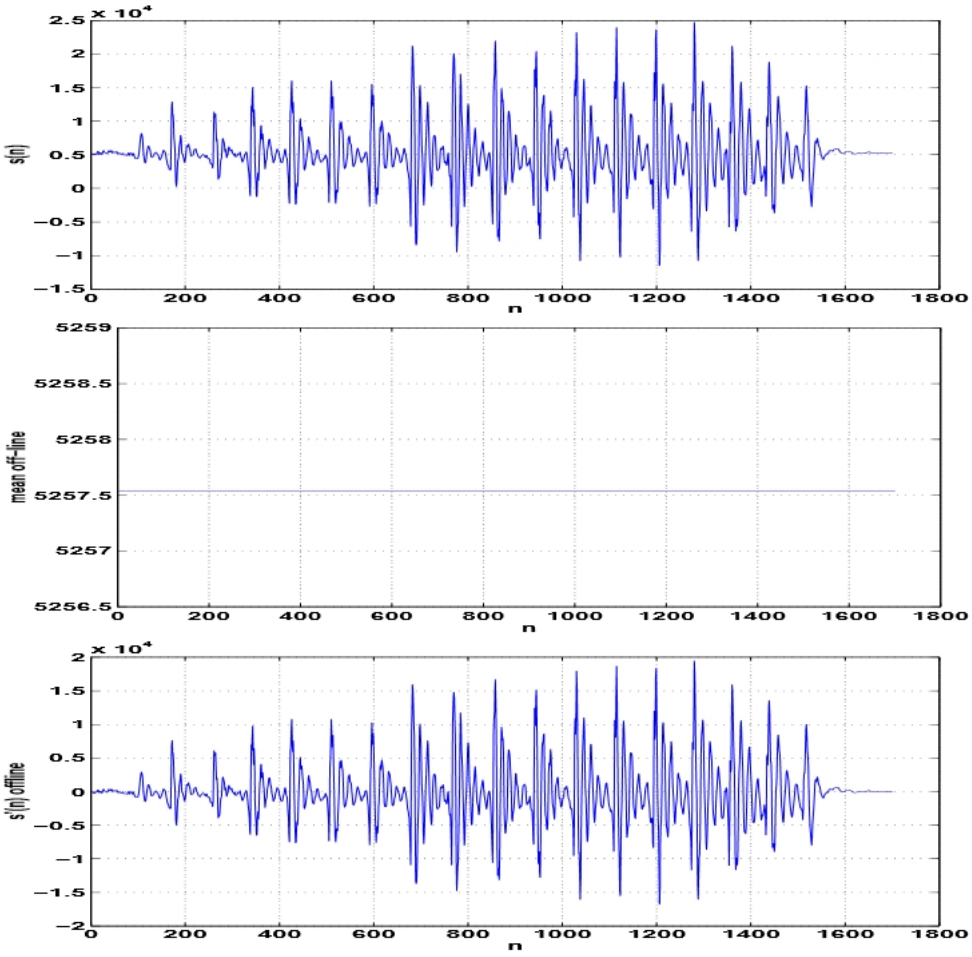

Figure 4.11: The offline mean value. From top to bottom: the original signal, the mean value, the signal after the subtraction of the mean value [13]

Online computation of mean value

If the signal is not available as a whole or the signal is still being received, it is possible to estimate the mean value recursively:

$$\bar{s} = \gamma \bar{s}[n-1] + (1-\gamma)s[n] \tag{4.17}$$

which is equivalent to the linear filter with the following impulse response:

$$h = [(1-\gamma)(1-\gamma)\gamma(1-\gamma)\gamma^2 \dots] \tag{4.18}$$

The result of such computation is shown in the figure 4.12

Segmentation

To analyse the radar signal, it is necessary to perform the segmentation of this signal. In other words, to divide the signal into individual frames. The reason for this is that the radar signal is random signal and is not stationary (its statistical parameters change over

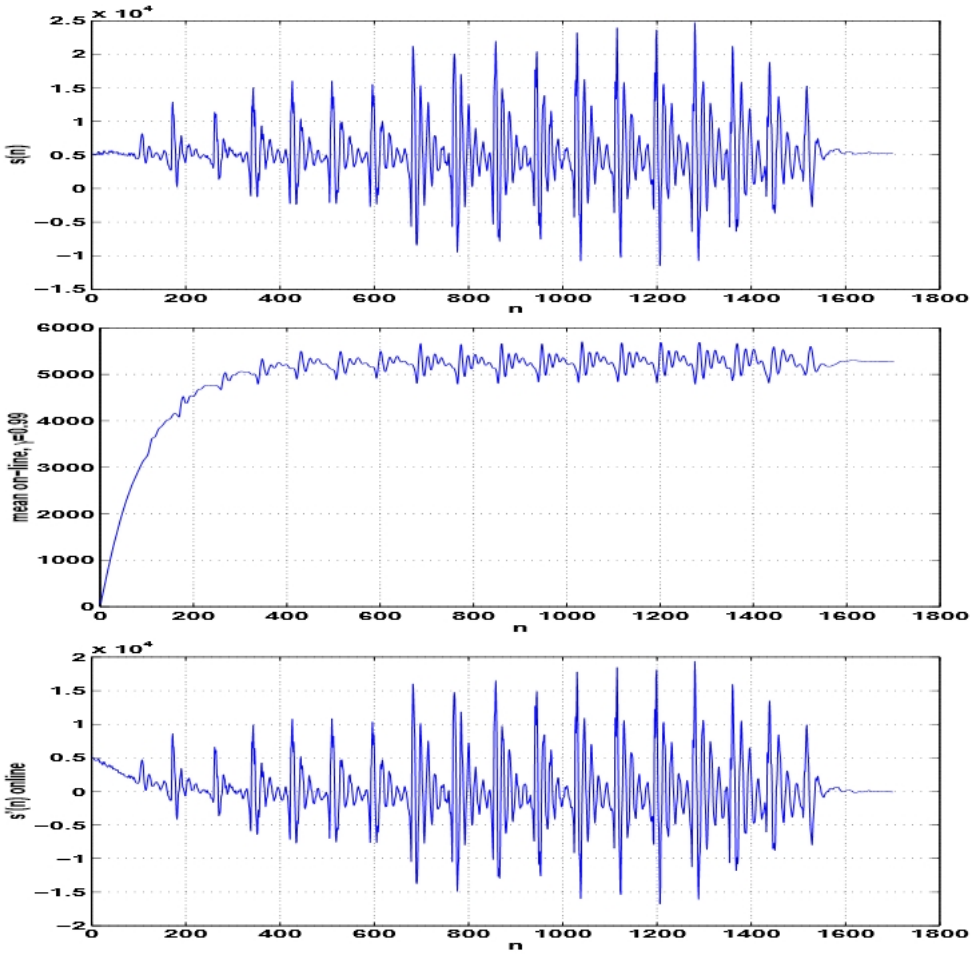

Figure 4.12: The online mean value. From top to bottom: the original signal, the mean value, the signal after subtraction of the mean value [13]

time). In order to analyse the signal, it is necessary need to analyse shorter sections of the signal, called segments or frames.

In general, the length of the segment should be „long enough“ to safeguard the ability to accurately estimate needed parameters and „short enough“ to maintain stationarity of the signal over the segment.

However, as our case is the radar signal processing of the frequency–modulated continuous–wave radar, our situation is a little bit easier. To determine the length of the segment, the simple length of the modulation sweep is computed. In the case of sawtooth modulation the modulation cycle is only upsweep, so the one segment contains the whole modulation cycle, in the case of triangular modulation, the modulation cycle is divided into two segments, one containing the upsweep of the modulation and the second one containing the downsweep of the modulation cycle.

In other situations, however, must be determined or estimated as a compromise between the „long enough“ and „short enough“ situations described above. What's more, it is also necessary to set the overlapping of individual segments, which can be of two kinds:

1. **a small or no overlap** low demands on processor and memory, a fast advancement in the signal (less segments to analyse), however the parameters of the individual segments may be rather different from each other.

2. **a big overlap** high demands on processor and memory, a slow advancement in signal (more segments to analyse), smoother changes of parameters over several segments. If the application requires analysis using Hidden Markov Models, the similarity of parameters between frames may be against the condition of the statistical independence.

Window functions

Window functions are used to perform the actual segmentation - to cut the part of the signal for analysis. However, multiplying the signal by the window function not only cuts the signal in the time domain, but also changes the spectrum of the cut signal, as the multiplying in the time domain corresponds to the convolution in the frequency domain, so the frequency characteristics of the window function are also important:

$$H(f) = S(f) * W(f) \tag{4.19}$$

The two most used window functions are the rectangular window and the Hamming window. The comparison is shown in the figure 4.13 :

1. **The rectangular window** this windows is defined as:

$$w[n] = \begin{cases} 1 & \text{for } 0 \leq n \leq length - 1 \\ 0 & \text{elsewhere} \end{cases} \tag{4.20}$$

   This window is more selective than the Hamming window, as it has the narrower central lobe (in the frequency domain), however it also changes the spectrum of the resulting signal more than the Hamming window because of its frequency characteristics.

2. **The Hamming window** is defined as:

$$w[n] = \begin{cases} 0.54 - 0.46 \cos \frac{2\pi n}{length-1} & \text{for } 0 \leq n \leq length - 1 \\ 0 & \text{elsewhere} \end{cases} \tag{4.21}$$

   This window is less selective (it has wider central lobe in the frequency domain), but it is better when it comes to the frequency characteristics because its spectrum has much weaker high–frequency components which do not change the resulting spectrum as much as in the previous case.

Discrete Fourier Transform

As mentioned in the previous chapter, in section 3.4, in order to gain information about the range to the target (height) and velocity of the target (vertical speed of the aircraft) it is necessary to compute the spectrum of the received signal and find the maximum of its absolute value.

To compute the spectrum of the signal a method called Fourier Transform is used (the equation 4.1), but, as our signal is discrete–time, a variant called Discrete Fourier Transform will be used.

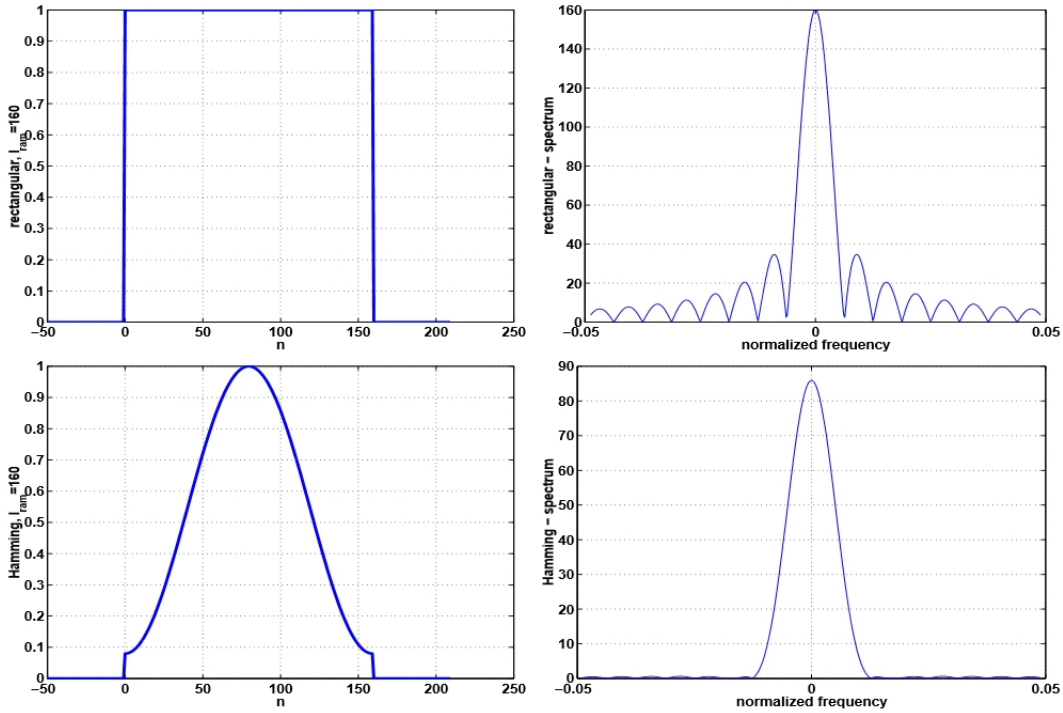

Figure 4.13: Window functions. Top: the rectangular window, Bottom: the Hamming window. Left: the time domain, Right: the frequency domain [13]

$$X(k) = \sum_{n=0}^{N-1} x[n] e^{-j2\pi \frac{nk}{N}} \text{for\_} k \in [0, N-1] \tag{4.22}$$

The DFT itself is a sequence rather than a function of a continuous variable. The DFT corresponds to the samples, equally spaced in frequency, of the Fourier transform of the signal. The DFT is the cornerstone of many signal processing algorithms and systems, because there are efficient algorithms how to compute it and also because of its properties (discussed more for example in [18]).

The major application is the analysis of the frequency content of the continuous–time signals like speech processing, where it is useful in identifying and modelling the resonances in vocal cavity, or in radar signal processing, where the velocity of target is represented by the frequency shift of the transmitted and the received signal (Doppler radar) and also to find the corresponding frequency for the computation of the range (FMCW radar) [18].

If the DFT is applied to the sampled signal (and only on the segment of the singal cut from the original signal by the window function), the spectrum with following characteristics is get:

- As the analysed signal is sampled, the spectrum is periodic with period N, which corresponds to the sampling frequency F_s.
- As mentioned in the description of the window functions, the spectrum is affected by the spectrum of the window function used to cut the segment from the original signal.

- The spectrum is discrete (like the spectrum of the periodic signal) and the number of frequencies in the signal is equal to the number of samples of the analysed signal. These frequencies are equally spaced in the interval $[0, F_s]$ with the step Δf:

$$\Delta f = \frac{F_s}{N} \tag{4.23}$$

where N is the number of samples of the analysed signal. Sometimes a higher resolution in the frequency is needed. A technique called **zero–padding** can be used to achieve this. The zero–padding „pads“ the original signal with additional zeros to make the N greater. It adds no useful information to the signal, but increases the number of frequency bins, thus making the spectrum „smoother“.

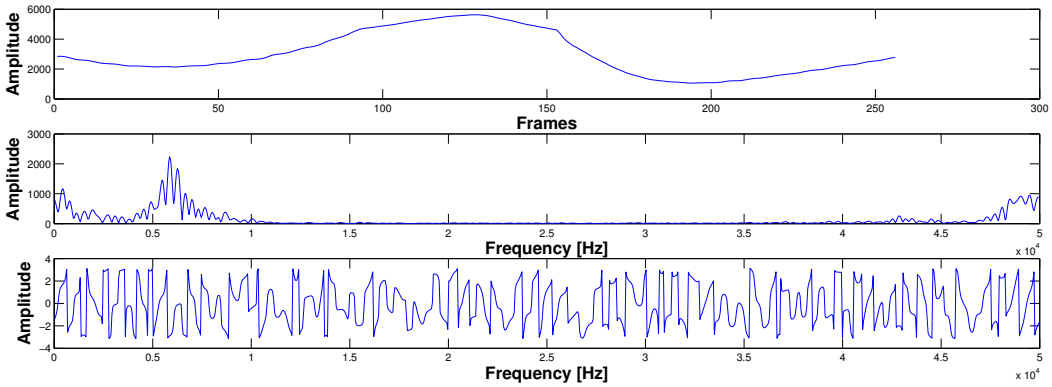

Figure 4.14: The DFT of the radar signal segment. From top to bottom: the radar signal (an absolute value, the signal itself is complex), the amplitude of the spectrum and the phase of the spectrum.

Efficient Computation of the DFT

As mentioned, the Discrete Fourier Transform is the basics of many signal processing algorithms and systems. One of the reasons is the fact that there are efficient algorithms how to compute it. These efficent algorithms may be divided into two classes [18].

The first one are algorithms that work well when the DFT values over only a portion of the frequency range $0 \leq \omega \leq 2\pi$ are required. In such case, these algorithms may be more efficient and flexible than the Fast Fourier Transform, but they are less efficient if all values of the DFT are needed. The example of such algorithms are Goertzel algorithm and the chirp transform algorithm [18].

The second class are algorithms collectively known as the Fast Fourier Transform. These algorithms are aimed at digital computation of the N–point DFT. To achieve the highest efficiency, these algorithms have to compute all the values of the DFT [18].

Fast Fourier Transform

The Fast Fourier Transform is based on the two properties of the DFT: the complex conjugate symmetry and the periodicity of n and k (see following equations). Its aim is to reduce the computation time needed for the direct computation of the DFT [18].

To compute each value of the DFT, N complex multiplications and $N-1$ complex additions are required to be computed, so for all N values, it is necessary to perform N^2 complex multiplications and $N(N-1)$ complex additions. It is clear that the computational time for bigger N can be significant (or the computation requires more computational power) [18].

The first algorithms using the symmetry and the periodicity properties of W_N^{nk} can be traced back to Gauss (1805). Then Runge in 1905 and Danielson and Lanczos in 1942 published algorithm which computations was proportional to $N \log N$. However, at that time the DFT was computed only for small N (as there were no computation means other than the hand computation) so the advantages of such algorithm were less important. The breakthrough came in 1965 when Cooley and Tukey published an algorithm that is applicable when the N is a composite number. Since then more efficient algorithms have been discovered, all collectively known as Fast Fourier Transform [18].

To better show the mentioned properties, let's rewrite the DFT equation into the more convenient form [18]:

$$X(k) = \sum_{n=0}^{N-1} x[n] e^{-j2\pi \frac{nk}{N}} = \sum_{n=0}^{N-1} x[n] W_N^{nk} \tag{4.24}$$

where

$$W_N = e^{-j2\pi \frac{nk}{N}} \tag{4.25}$$

Then the complex conjugate symmetry is:

$$W_N^{k[N-m]} = W_N^{-nk} = (W_N^{nk})^* \tag{4.26}$$

and the periodicity in n and k is:

$$W_N^{nk} = W_N^{k[n+N]} = W_N^{[k+N]n} \tag{4.27}$$

There are two approaches which are used in FFT algorithms: the decimation–in–time and the decimation–in–frequency. The decimation–in–time algorithms are based on decomposing the sequence $x[n]$ (input) into succesively smaller sequences. The decimation–in–frequency algorithms are based on dividing the output sequence $X(k)$ into smaller and smaller subsequences in the same manner [18].

Decimation–in–time

The principle of the decimation–in–time algorithm is best described when considering the special case of N–point DFT where N is an integer power of 2. This algorithm exploit both the symmetry and periodicity properties of the DFT [18].

As the N is an even number it is possible to compute $X(k)$ by dividing $x[n]$ into two separate (N/2)–point sequences, where in one sequence there are even–numbered points in $x[n]$ and the odd–numbered points in $x[n]$ are in the other one [18].

Let us consider the equation 4.24. After the separation of $x[n]$ into its even– and odd–numbered points we get [18]:

$$X(k) = \sum_{n\_even} x[n] W_N^{nk} + \sum_{n\_odd} x[n] W_N^{nk} \tag{4.28}$$

With the substitution of variables $n = 2r$ for even number and $n = 2r + 1$ for odd numbers we get:

$$\begin{aligned} X(k) &= \sum_{r=0}^{(N/2)-1} x[2r] W_N^{2rk} + \sum_{r=0}^{(N/2)-1} x[2r+1] W_N^{(2r+1)k} = \\ &= \sum_{r=0}^{(N/2)-1} x[2r] (W_N^2)^{rk} + W_N^k \sum_{r=0}^{(N/2)-1} x[2r+1] (W_N^2)^{rk} \end{aligned} \tag{4.29}$$

The $W_N^2 = W_{N/2}$ because:

$$W_N^2 = e^{-2j(2\pi/N)} = e^{-j2\pi(N/2) = W_{N/2}} \tag{4.30}$$

so we can write:

$$X(k) = \sum_{r=0}^{(N/2)-1} x[2r] W_{N/2}^{rk} + W_N^k \sum_{r=0}^{(N/2)-1} x[2r+1] W_{N/2}^{rk} \tag{4.31}$$

and with denoting the sums $G[k]$ and $H[k]$, respectively:

$$X(k) = G(k) + W_N^k H(k), k = 0, 1, \ldots N-1 \tag{4.32}$$

Both sums $G[k]$ and $H[k]$ are recognized as the (N/2)–point DFT, the first sum being the (N/2)–point DFT of the even–numbered points of the original sequence and the second sum being the (N/2)–point DFT of the odd–numbered points of the original sequence. Although the index k ranges over N values, both sums must be only computed only for k between 0 and $(N/2) - 1$ because they are both periodic with period $N/2$. After both DFTs are computed, they are put together to yield the N–point DFT (equation 4.32) [18]. This is shown in the figure 4.15. This technique reduces the number of required computations from N^2 to $N + N^2/2$ for $N > 2$ [18].

However, if the $N/2$ is even number, which it is provided that N is a power of 2, the process can continue and the (N/2)–point DFT can be computed as two (N/4)–point DFTs and so on. The 8–point DFT shown in the figure 4.15 can be then computed using only the 2–point DFTs (the figure 4.16). After carrying out as many decompositions as possible the number of complex additions and multiplications is equal to $N = N \log_2 N$ [18].

Decimation–in–frequency

The principle of the decimation–in–time algorithm is again best described when considering the special case of the N–point DFT, where N is an integer power of 2. The decimation–in–time algorithm use the division of the input sequence $x[n]$. The decimation–in–frequency uses similar approach, but divides the output sequence $X(k)$ into the smaller and smaller subsequences [18]. Let us consider the equation 4.24. After the separation of $X(k)$ into its even– and odd–numbered samples we get for the even–numbered samples [18]:

$$X[2r] = \sum_{n=0}^{N-1} x[n] W_N^{n(2r)}, r = 0, 1, \ldots, (N/2) - 1 \tag{4.33}$$

which can be rewritten as:

$$X[2r] = \sum_{n=0}^{(N/2)-1} x[n] W_N^{2nr} + \sum_{n=(N/2)}^{N-1} x[n] W_N^{2nr} \tag{4.34}$$

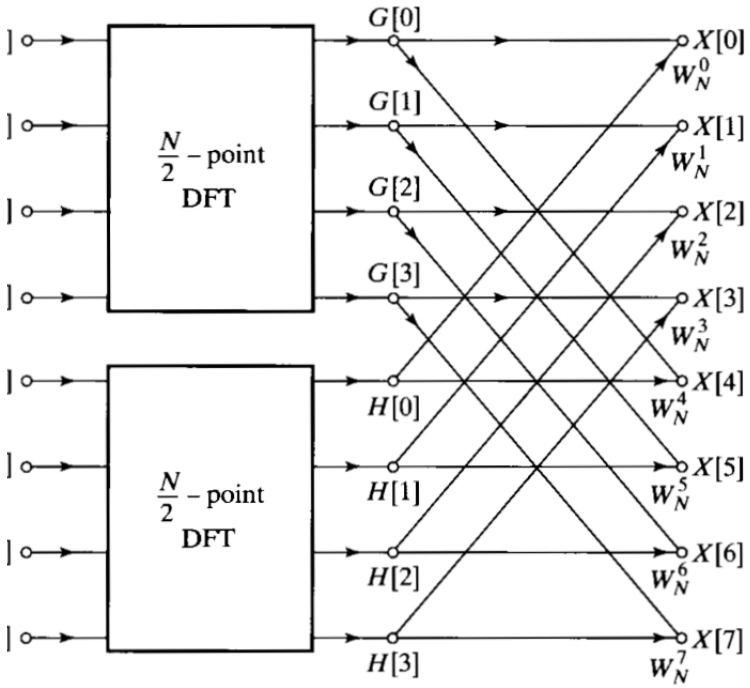

Figure 4.15: Decomposition of the 8–point DFT into the two (N/2)–point DFTs. Nodes denote the summation [18].

With the substitution of variable in the second sum we obtain:

$$X[2r] = \sum_{n=0}^{(N/2)-1} x[n]W_N^{2nr} + \sum_{n=(N/2)}^{N-1} x[n+(N/2)]W_N^{2r[(n+(N/2)]} \tag{4.35}$$

Then, because of the periodicity of W_N^{2rn}:

$$W_N^{2r[(n+(N/2)]} = W_N^{2rn}W_N^{rN} = W_N^{2rn} \tag{4.36}$$

and because of 4.30, the equation 4.35 can be expressed as:

$$X[2r] = \sum_{n=0}^{(N/2)-1} (x[n] + x[n+(N/2)])W_{N/2}^{rn}, r = 0, 1, \ldots, (N/2) - 1 \tag{4.37}$$

The previous equation is the (N/2)–point DFT of the (N/2)–point sequence obtained by adding the first half and the last half of the input sequence. This addition represents time aliasing because the computation of only the even–numbered frequency samples undersamples the Fourier transform of $x[n]$. The odd–numbered points are obtained similarly, the result being [18]:

$$X[2r+1] = \sum_{n=0}^{(N/2)-1} (x[n] - x[n+(N/2)])W_N^n W_{N/2}^{rn}, r = 0, 1, \ldots, (N/2) - 1 \tag{4.38}$$

The previous equation is the (N/2)–point DFT of the (N/2)–point sequence obtained by subtracting the second half of the input sequence from the first half of the input sequence

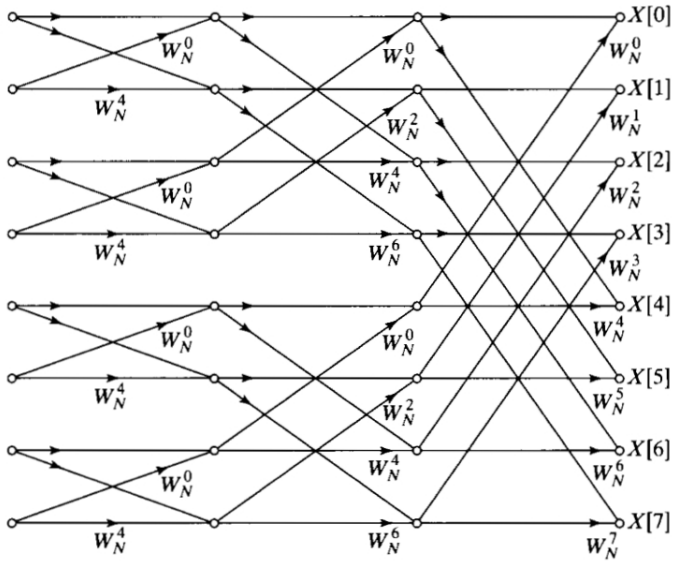

Figure 4.16: Decomposition of the 8–point DFT into 2–point DFTs. Notes denote summation [18].

and multiplying the result by W_N^n [18]. If we substitute this subtraction and previous addition as:

$$g[n] = x[n] + x[n + (N/2)]; \_h[n] = x[n] - x[n + (N/2)] \tag{4.39}$$

then the DFT can be computed first by computing these sequences, then by multiplying $h[n]$ by W_N^n and then computing (N/2)–point DFT to gain even– and odd–numbered points [18]. This is illustrated in the figure 4.17. As in the previous case of the decimation–in–time

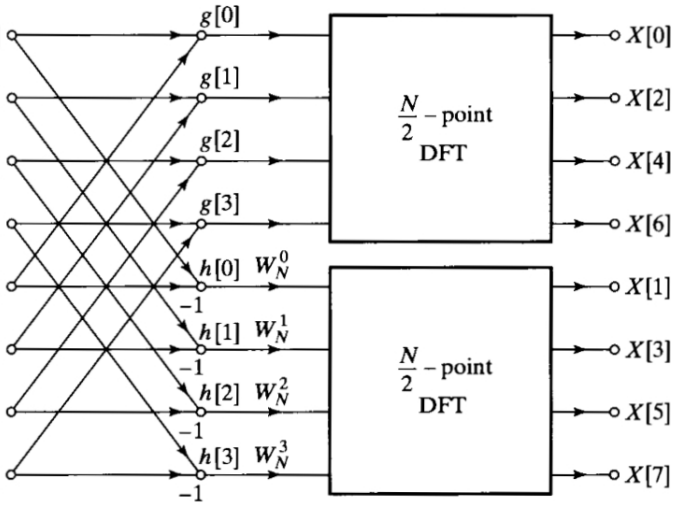

Figure 4.17: Decomposition of the 8–point DFT into two (N/2)–point DFTs. Nodes denote the summation [18].

technique, the decimation–in–frequency can too continue by computing the (N/2)–point DFT by computing two (N/4)–point DFT and so on [18]. The figure 4.18 shows the complete decomposition.

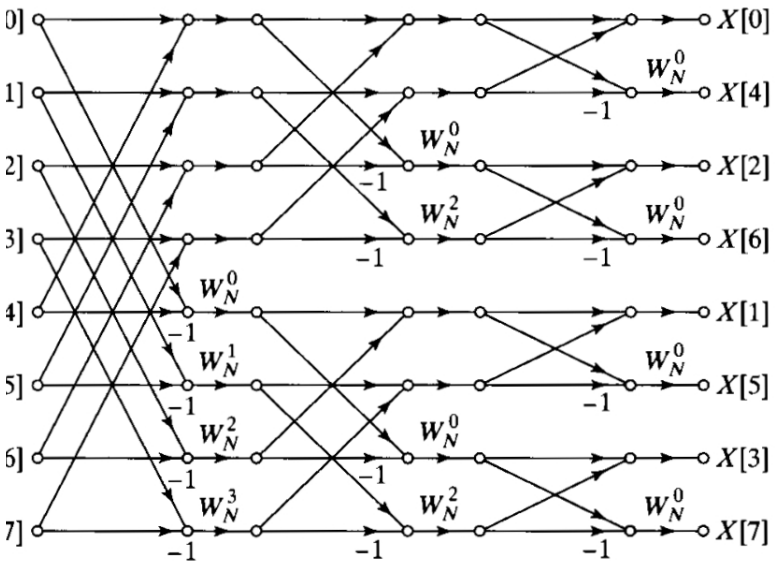

Figure 4.18: Complete decimation–in–frequency decomposition of the 8–point DFT. Nodes denote summation [18].

The decimation–in–frequency has a similar speed–up of the computation of the DFT as the decimation–in–time. It requires $(N/2)\log_2 N$ complex multiplications and $N\log_2 N$ complex additions [18].

Because of the described speed–up, the Fast Fourier Algorithms are widely used, which led also to the widespread support of them in various computation software like the Mathworks Matlab or several paid or free libraries for general–purpose languages like the C/C++ languages.

Chapter 5

Analysis and solution proposal

The aim of this thesis is to create an algorithm for signal processing of the frequency–modulated continuous–wave radar, which could be used as a processing algorithm in the radio altimeter for light aircraft. The purpose of such radio altimeter is to make the landing manoeuvre easier and safer for the pilot and passengers onboard. Therefore, the focus is on the real–time capability and the sufficient accuracy so as to provide the pilot with up–to–date and quality data about the height above the ground and, if possible, also about the vertical speed of the aircraft. Even though such devices already exist, they are primarily used in bigger, commercial airliners or business aircraft (or, of course, military airplanes) and are yet to be widely used in general aviation.

Possible target platforms

As the digital signal processing is the current state–of–the–art approach to signal processing and analog signal processing may be considered outdated, only digital platforms will be considered. Some of the following features were adapted from [17].

Personal computer

The personal computer is one of the possible target platforms. Being the most universal device, it has the following features:

- Generally high computational power (even though depending on used components).
- A possibility to perform any needed computation (PC is a general–purpose device, usually utilizing x86 CPU).
- A possibility to use many operating systems.
- A possibility to use and compile any programming language, be it compiled or interpreted one.
- A possibility to run applications with graphic user interface.
- Higher cost, higher energy consumption.

Embedded system or SoC

The embedded systems may be considered as a cost and energy effective alternative alternative to the PC:

- A possibility to perform any needed computation (embedded system is a general–purpose device, usually utilizing ARM CPU)
- The usage of operating systems.
- Operating systems choice are usually limited to Linux distributions
- Generally less computational power than the PC has.
- Can be programmed in high–level programming languages, usually C or C++ (the same code as on the PC).
- Lower cost and generally low energy consumption.
- Current commercially available devices often provide an FPGA which may be used for speed–up of computations.

FPGA

Field–programmable gate array may be considered a hybrid between the general–purpose devices such as the personal computer or the embedded system and application specific integrated circuit.

- The possibility to programme hardware at low–level.
- Possibly very low energy consumption.
- The programming in VHDL/Verilog or C-like languages. (CatapultC).
- The parallel computing.
- Very often used together with the embedded system for speed–up of time–crucial tasks.

ASIC

The last possible option is the ASIC (Application specific integrated circuit)

- The most energy efficient and powerful solution.
- The highest cost.
- Errors in design are far more costly than the other platforms.
- Suitable only for mass production, which reduces cost of one chip.

Solution proposal

Of all these options, considering their features, the embedded system seems the most suitable for the task. It provides almost all of the features of the personal computer, but with the reduced cost and energy consumption. The crucial feature is the possibility to develop, optimize and debug the code using the personal computer and then transfer the code to the embedded system with possible speed–up of crucial time–consuming tasks using the built-in FPGA. Moreover, the development on the PC can be speeded up by using computing software suitable for signal processing such as Mathworks Matlab and then converting the code into the pure C/C++ form. From all available embedded systems (or SoCs), Xilinx Zynq-7000 will be used.

The algorithm itself will implement the signal processing of the frequency–modulated continuous–wave radar with sawtooth modulation. The selected method of signal processing is 2D Discrete Fourier Transform described in the previous chapter with the usage of common signal pre-processing techniques. If the information about the Doppler frequency is not needed in the final product or could be obtained using different approach (such as the triangular modulation of the frequency), a simple 1D DFT may be used instead. The algorithm will be developed firstly using the Matlab software and later, if the time permits, transferred into the dedicated C/C++ code. As the goal is the signal processing for radio altimeter used during landing manoeuvre, the primary focus will be on real–time capability and accuracy (especially for low–height situations). The possible problem that might occur could be the impossibility to achieve this goals on the selected platform. A solution to this problem is the change of the target platform (or version) or the change of the signal processing method. However, the goal is to keep the algorithm as simple as possible.

Xilinx Zynq

Xilinx Zynq is a series of all–programmable System–on–chip devices produced by Xilinx. The following is the summary of the Xilinx Zynq-7000 Product Brief [9]. The series is divided into two classes: Zynq-7000S devices, which are equipped with single core CPU and Zynq-7000 devices, which are equipped with dual core CPU. Regardless of the number of cores, the used CPU is ARM-Cortex A9, with up to 1GHz operational frequency and single and double precision floating point support.

Xilinx Zynq has 512kB L2 Cache memory, 256kB On-Chip memory for operating system and memory controllers support up to DDR3-1866. The device is equipped either with the low–power and low–cost Artix-7 28 nm FPGA or high–performance Kintex-7 28 nm FPGA. The ports of the device include two USB 2.0 ports, Gigabit ethernet port, UART and SPI.

Operating systems available are Linux for the general–purpose computing, FreeRTOS for simple high–performance tasks, Bare–Metal for the low–level high–performance applications and Android for applications with graphical user interface.

Mathworks Matlab

Matlab (abbreviation for MATrix LABoratory) is a high–level programming language and interactive environment for numerical computation and technical computing, visualisation and programming developed by MathWorks company [14].

Matlab is widely used computational tool in science and engineering, encompassing fields of mathematics, physics, chemistry and all engineering streams. Its main usages include: signal processing and communication, image and video processing, control systems, test and measurement, computational finance and computational biology [10].

Matlab has a sophisticated data structures, the basic data element is an array that does not require dimensioning, it supports object-oriented programming, has built-in editing and debugging tools, and provides application packages, called toolboxes, for specific usage purposes mentioned above [14]. These are the advantages of Matlab over conventional programming langauges, such as the C language. As such, Matlab may be considered standard and state–of–the–art tool for technical computations in education, research and industry [14].

Implementation requirements

There are several requirements which the implementation of the algorithm should meet to provide a solution feasible for the radio altimeter:

- The algorithm should process the triangular frequency–modulated signal, because of the available test data and general useful properties of such modulation pattern.
- The algorithm should be able to run on the selected target platform in real–time. The exact computation time is hard to define, but the outputted data should not noticeably lag behind the reality.
- The error in the height computation of the algorithm should be below 1 m, ideally below 0.5 m.
- The minimum detectable height should be 1 m or less, the maximum detectable height should be 30 m or more.
- The intended use of the radio altimeter is to help the pilot with the landing of the airplane. Because of this, the performance of the algorithm for the landing phase of the flight has the priority.

The implementation of the solution with respect to these requirements is described in the next chapter.

Chapter 6

Implementation

The radar signal processing algorithm has been developed and written in Matlab environment. The algorithm uses pre-recorded radar output data to compute the height above the ground level of the radar module (and thus the aircraft). In the previous chapter, a 2D Fourier Transform has been proposed as a suitable signal processing method. However, as the available radar data contain signal modulated with triangular wave, rather than the simple sawtooth, the Doppler frequency may be computed directly from standard 1D Fourier transform, so the 2D Fourier transform method is not needed. Moreover, the vertical velocity information is not required in this application, so the Doppler frequency is used purely to correct the measured height by adjusting the frequency with respect to the Doppler shift.

6.1 Radar Data

To develop the algorithm, a real–world radar data were used. The algorithm was tuned primarily on the data containing the whole flight, including the take–off and landing. In the available data set, only two such flights were included. Therefore, in order to use this algorithm in commercial product, further test with additional data are needed to fine–tune the parameters and safeguard the functionality in all situations.

Radar Module

The radar sensor used in test flights was IVS-948 produced by German company called InnoSennT. The supporting hardware completing the radar module has been produced by Czech company CAMEA.

The radar sensor IVS-948 is a K–band transceiver. It is the advanced version of the IVS-148 model and is primarily aimed at traffic monitoring and industrial applications. It features 1/x divider for the reference frequency output, stereo operation to detect the direction of motion, an integrated RF–pre–amplifier, programmable IF-amplifier and two selectable power outputs. It can operate in Continuous–wave mode (CW), Frequency–modulated continuous–wave mode (FMCW) and Frequency–shift keying mode (FSK). Using this sensor, it is possible to gain information about the presence, movement, distance, velocity and direction of the target. It is not possible to detect the angle, however [6]. The parameters of the radar signal, important from the point of view of the signal processing, are summarized in the following table.

Figure 6.1: IVS-948 radar sensor [7].

Gain	Value
Mode	FMCW
Modulation Pattern	Triangular
Modulation Frequency	$0.26\,Ghz$
Modulation Period	$5.12 \times 10^{-3}\,s$
Sampling Frequency	$5 \times 10^{3}\,Hz$
Samples per Period	256

Table 6.1: Radar signal parameters.

6.2 The Algorithm

The developed algorithm itself consists of four parts:

Radar signal preprocessing and FFT

The radar signal preprocessing starts with getting the one segment from the radar data, which corresponds to the one modulation period, in other words it contains one „triangle“.

Firstly, the real and imaginary part of the sampled signal are divided. Then, the DC component is subtracted from both parts by simple subtraction of the mean value.

Secondly, both real and imaginary parts are divided into two parts: the one which corresponds to the upsweep part of the modulation cycle („the rising edge of the triangle“) and the one which corresponds to the downsweep part of the modulation cycle („the falling edge of the triangle“). For both parts, first five percent of the modulation sweeps are omitted to avoid unstability of signal after the sweep direction change.

Subsequently, all these four parts of the signal are multiplied by Hamming window and then real and imaginary parts of the upsweep and the downsweep parts of the signal are merged into complex numbers, effectively creating two signal segments to analyze, which are processed by 1024–point Fast Fourier Transform (actual signal with the zero padding).

Even though these preprocessing steps are important, they can be considered standard. However, during the development, a need for another preprocessing method has arised as all of the spectrums (meaning spectrums of all segments throughout the entire signal), produced by Fast Fourier Transform, contained dominant parasitic peak at low frequencies (broadly comparable to the range of one metre). The source of this peak is unknown, but it is probably caused by the beat phenomenon.

This peak not only made it impossible to detect low–frequency „useful“ peaks, but was also so dominant (the difference of amplitudes between this and the sought peaks was up to 10^4), that all useful peaks were virtually non–existent and impossible to find. An example of such spectrum is shown in the figure 6.2.

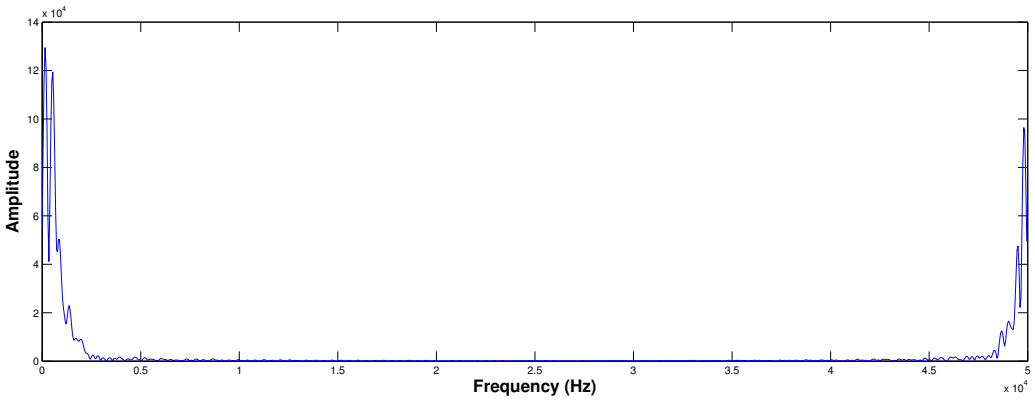

Figure 6.2: An example of spectrum with parasitic peaks.

Therefore, several methods how to cope with this problems were experimented with. The conducted experiments have shown that the best way (at least from those tested) is to subtract the average of the several previous spectrum (the spectrums of the previous signal segments) from the currently analysed one. The efforts to use long–term average „noise“ spectrum (gained from the spectrums of segments, when there was no target and thus no corresponding radar response) proved unsuccessful and had little to no effect. This is caused by the fact, that the phase of the signal slightly changes, albeit slowly, so the subtraction of the spectrums with the same or similar phase, which are close to the current one in the time domain, is more effective. The resulting spectrum is shown in the figure 6.3.

Frequency peak finding

After both spectrums are gained, the spectrum for the upsweep part of the modulation cycle is flipped, and added to the spectrum of the downsweep of the modulation cycle. By doing so, the peaks can be searched for only in one resulting spectrum.

The flip of the upsweep spectrum is done because the location of range peaks in this spectrum was the upper half of the spectrum, whilst range peaks in the downsweep spectrum were in the lower half. Because of that, by adding the two spectrums together not only produces only one spectrum to search for the peaks in, but the search can also be conducted only in the lower half of the spectrum. The illustration is shown in the figure 6.4.

As the two spectrums are added together, the algorithm searches for two peaks. Corresponding frequencies are then determined for the found peaks and the average of these

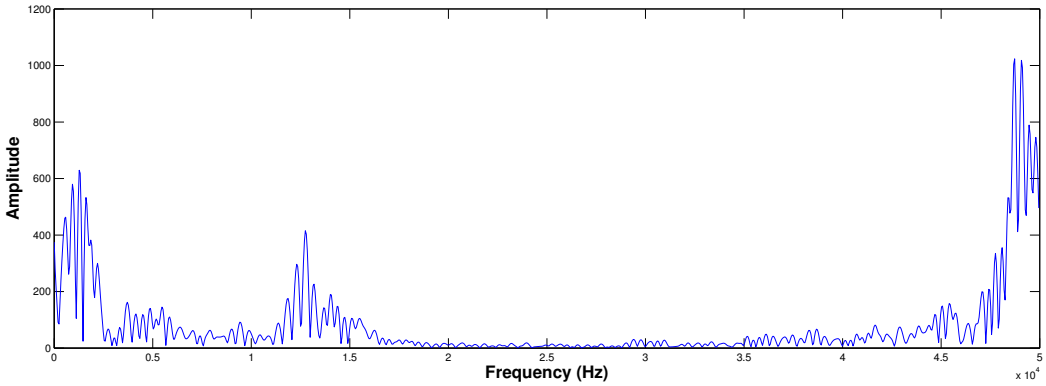

Figure 6.3: An example of the spectrum with range peak at approximately 12KHz.

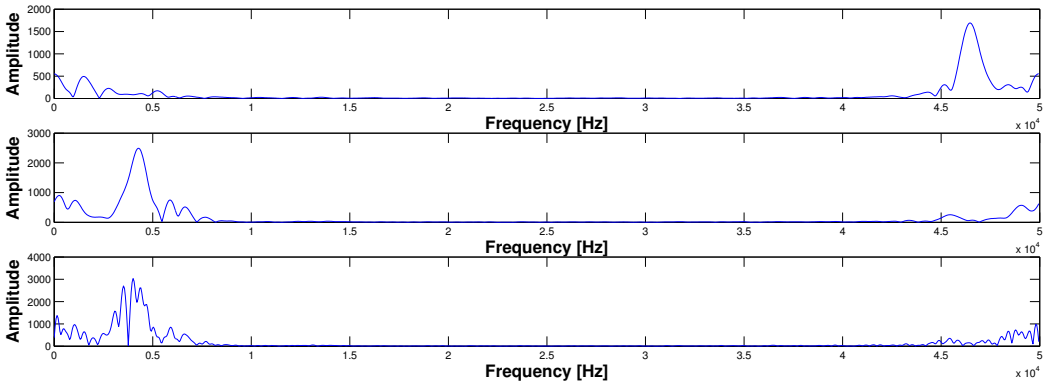

Figure 6.4: The flip of the spectrum. From top to bottom: the rising edge spectrum, the falling edge spectrum and the resulting spectrum.

two frequencies is used as a frequency for the range computation, eliminating the Doppler frequency. However, the process of finding the right peaks is not so straightforward.

Take-off and ascend

Firstly, as mentioned in the previous section, there is a parasitic peak in the data spectrums. Even though the subtraction of the average of several previous spectrums helped the case, the parasitic peak is still present, albeit with much lower amplitude.

Fortunately, experiments have shown that this peak has more or less steady both position and amplitude, so extra methods during the peak finding could be employed to overcome this situation.

The first technique used is the variable starting position of the search for the range peak. As mentioned in previous section, a 1024–point Fast Fourier Transform is performed and range peaks occur only in the first half of the spectrum so the standard search for the range peaks is conducted between positions 1 and 512 of the spectrum. However, the parasitic peak still has a non–negligible amplitude and tests have shown that range peaks (at least in the test data) are more dominant only for ranges up to approximately 13 metres, although

they are of course present in spectrum for higher ranges as well. To enhance the high range detection capabilities of the algorithm, a solution to this was needed.

The first idea was to detect not the highest peaks, but „other ones“, but this proved difficult to implement, as there was no way to determine, how high in the order of found peaks the right one would be for particular frame because the parasitic peak is often accompanied by several nearby peaks, which are parasitic as well.

The second idea proved itself as much more feasible way to solve this. When the average detected range crosses the `lowSeekThresholdRange` (10 metre mark; currently, 50 last frames are used for this average), the starting position (`lowSeekThreshold`) of the search is moved from 1 to 40 (40 for the 1024–point Fast Fourier Transform, for the FFT with different length, this number would have to be adjusted accordingly). A hypothetical peak at the position 40 corresponds to frequency approximately 1900 Hz, which corresponds to the height above the ground of approximately 5.6 m. This position has been determined experimentally, so that the search from this position onwards omits parasitic peaks at the beginning of the spectrum and also provides reserve in the search space should the aircraft descend immediately after triggering this change in the starting position of the search. If the average detected height descend below the `lowSeekThresholdRange`, the starting position of the search is reverted back to 1.

This method proved so successful that a third starting position has been introduced at the `highSeekThresholdRange` (30 metre mark), where the starting position moves to the position `lowSeekThreshold` (300). As in the previous case, this number was set for the 1024–point FFT and for the different FFT length it would have to be adjusted accordingly. This third position (1, 40 and 300) helps to detect high–frequency low–amplitude range peaks almost to the very end of the spectrum, corresponding to very high ranges (up to 62 metres for the test data). As the radar response for such ranges is rather unstable and also weak to the point that it is hard to tell apart from the noise, a safety measure was introduced to safeguard that the algorithm will not start finding noise peaks near the starting position of the search and consider them to be sought range peaks. This measure is a simple threshold (set experimentally). When the amplitude of the found peak falls below this threshold, the starting position is reverted immediately back to 1. This measure was also introduced for the second starting position (reverting from `lowSeekThreshold` to 1).

The figure 6.5 shows the output of the algorithm for the take–off phase of the flight number 1 without this feature. The maximum detectable height is very low, when compared to the results achieved with this feature (see the figure 7.2 for comparison).

No response detection

When the aircraft is flying in such height above the ground that it is beyond the range of the radar sensor, it is necessary to detect such situation and indicate it. The spectrum of the signal in such situation is of course not empty, but contains noise and already mentioned parasitic peak. As stated before, the amplitude and position of this parasitic peak is more or less steady so it can be taken advantage of and, if only such peak is found, used as an indicator, that radar sensor is not picking up any useful response from the target (which is the ground in this case). The algorithm then outputs zero height.

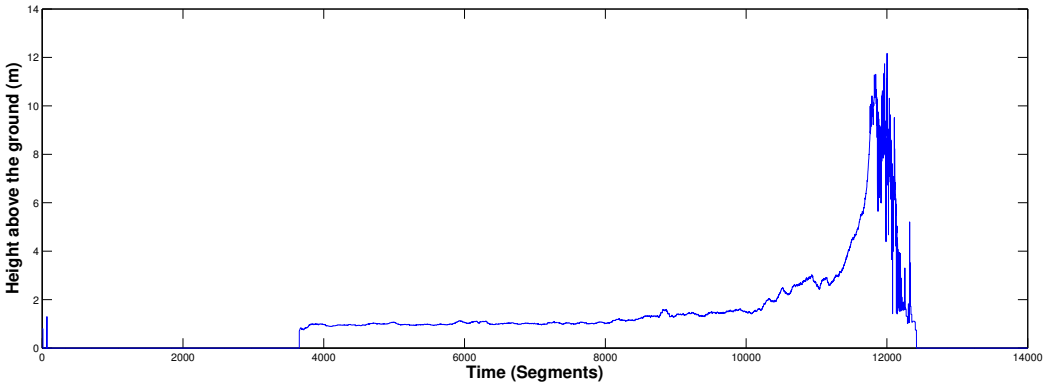

Figure 6.5: The take–off of flight number 1 without moving the starting position of the peak search.

Landing or descending

The technique described above proved to work well, but relies on the average of the detected height (range), which in case of altimeter means, that it works only for take–off of the aircraft or generally for the ascend of the aircraft. That caused that maximum detectable height above the ground was higher for take–off (or ascend) than for the landing (when the aircraft descends from the height which is not detectable by the used radar sensor) as the high–frequency low–amplitude peaks were „overshadowed“ by low–frequency parasitic, noise peaks.

A method to enhance the maximum detectable height of this algorithm was therefore designed and implemented. When the algorithm detects only parasitic peaks and assumes that it is not picking up any useful data, it deliberately checks for peaks in the upper half of the spectrum and if there are any peaks with above–the–threshold amplitude it considers them to be peaks caused by the response from the ground. As soon as such peaks are detected in enough number of subsequent segments, the average detected height triggers the shift of the starting position of the search in the spectrum described above and the detection method is the same as during the ascend, only now the computed height steadily decreases causing the starting position of the search to decrease as well. As there may be a desire to output height data only after the response is stable, this feature can be turned off.

One peak detection

As mentioned above in the section 6.2, the two spectrum are added together so the search is conducted for two peaks, which corresponding frequencies are then averaged to gain the on for the height computation. During the tests however, it sometimes happened that only one peak was detected for the expected height, or, to say it better, the difference of positions of the two found peaks was beyond the difference which could be justified by the Doppler shift. The reasons for this are that sometimes the noise peak was wrongfully detected or that the useful peak was missing at all.

This caused the drop in the computed frequency in some segments, which of course negatively affected the computed height. Therefore, when such situation occurs, only the peak at higher position in the spectrum is used for the height computation.

Radar signal post–processing and height computation

After the height is computed, a two post–process methods are used:

Adaptive output averaging

The original computed height data proved to be rather unstable so an average of the last computed heights is used as an output. After testing several values, 100 last values proved to be feasible number for the averaging window `numOfAvgSteady`. However, it caused the significant change of the steepness of slopes in data (for example during the climb or the descent of the aircraft) so when such situation is detected (computed by simple difference between computed heights of segments) a shorter averaging window `numOfAvgSlope` (20 segments) is used. It should be noted that the average is computed from actually computed values not outputted ones (outputted value may be different from the computed one, but in the subsequent segments the computed value is used in computation of the next outputted value). The figure 6.6 shows the output without averaging. It is clear that the outputted data are very unstable and some kind of smoothing is necessary (see the figure 7.2 for comparison with the averaged output).

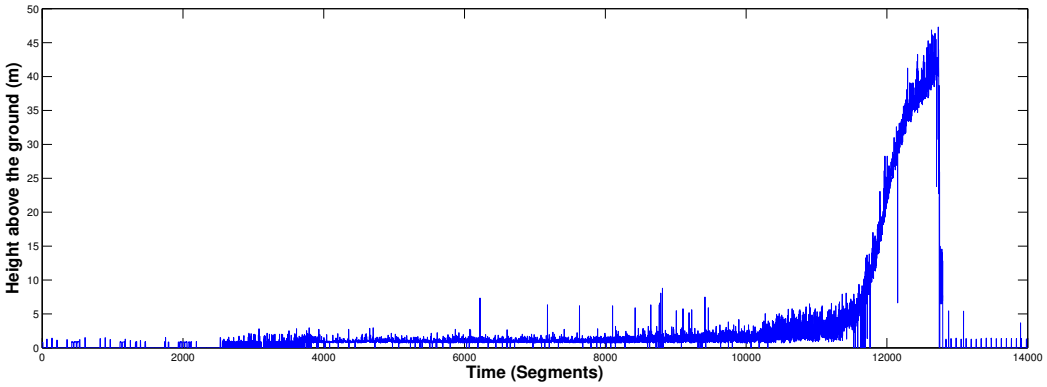

Figure 6.6: The take–off of flight number 1 without utilizing the average.

Output threshold

Because of the averaging mentioned above and thresholding the amplitude, it sometimes happened that a noise peak was higher than the threshold level and together with the averaging caused a very low height to be outputted (below the theoretical capability of the radar sensor). Because of this a threshold level for output level (set at $0.7\,m$) was introduced and if the output is below it, it is set to 0.

It should be noted that all thresholds, starting positions, window lengths etc. mentioned in this chapter are implemented as constants and thus can be easily changed to fine–tune the algorithm should more test data are available or a specific working conditions of the real–world product are known.

Chapter 7

Achieved Results

This chapter provides the reader with achieved results of the algorithm (see chapter 6.2 for the detailed description). The available data consisted of two „full flights“ which included pre–flight movement of the airplane, the take–off, the climb to the such height above the ground that it was outside the capabilities of the radar sensor to measure it and then the descent and subsequent landing of the airplane. The figure 7.1 shows the results achieved

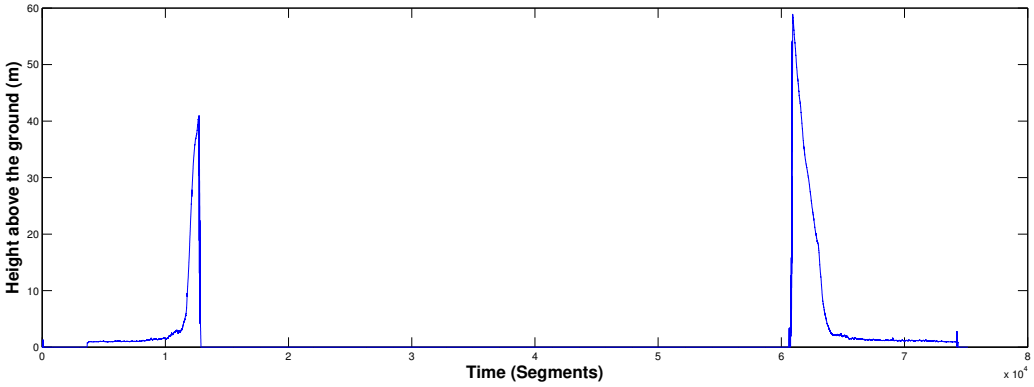

Figure 7.1: The complete flight number 1.

for the flight number 1. The x–axis represents time, measured in segments of the signal (one segment of the signal is equivalent to $5.12 \times 10^{-3}\,s$), whilst the y–axis represents the computed height above the ground (AGL - above the ground level in aviation glossary), measured in metres.

To better comment the achieved results, a detailed views of the take–off and the landing phase are provided in figure 7.2 (the take–off phase) and figure 7.3 (the landing phase).

7.1 The take–off

The beginning of the take-off phase (figure 7.2) shows that the response that the radar sensor picked up was evaluated as noise and therefore the algorithm outputs zero. Analyzing the raw Fourier Transform data for this phase showed that the response has been extremely unstable, both in the frequency and the amplitude and if not for averaging described in the section 6.2, there would be significant peaks in measured height. The reason for this

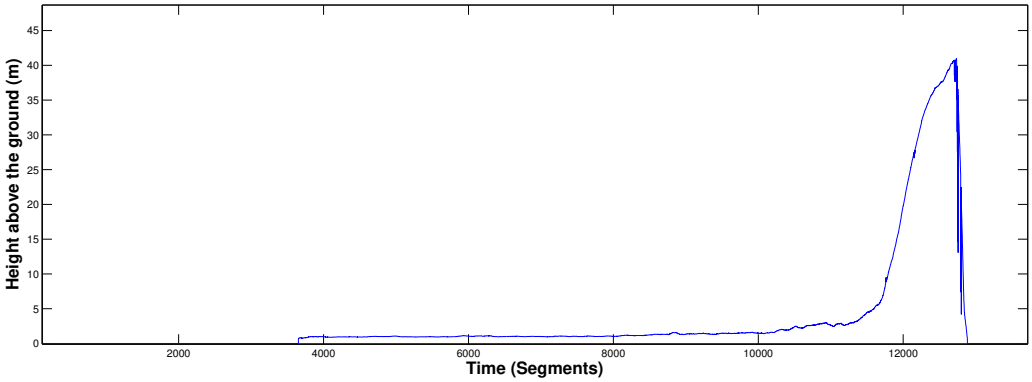

Figure 7.2: The take–off phase of the flight number 1.

is unknown, but the possible causes are some unstabilities caused by switching on the electronic device (the mentioned extremes in data were primarily at the very beginning of the measurement and gradually decreased) or the manipulation with the airplane before the actual flight (towing the airplane from the hangar, rotating it and so on).

After this phase, the response stabled at approximately 1 metre of height, where it held for a longer period of time, indicating the ground movement of the airplane. Unfortunately, the data were not accompanied with the information about the exact mounting height of the radar module so it is not possible to verify this or calibrate the algorithm to show „0“ in such situation.

Subsequently, the measured height rose by a relatively small amount, which most probably corresponds to the take–off itself and following flight at the low height to gain enough airspeed to commence the initial climb.

The climb itself is then the most visible part of the shown data, the airplane is steadily gaining height to the point where the radar sensor is not capable of measuring it.

The output of the algorithm then drops to zero, as the response is considered to be only noise. The drop is not imminent because of the averaging (6.2), which is the main problem of this method. There have been efforts to address this problem, but none of them was robust and usually „damaged“ the outputted data also in the other parts of the flight.

The data were not provided with any kind of ground–truth reference, however, the outputted data correspond to the standard take–off and post take–off movement of the airplane and therefore could be deemed (with the reasonable confidence level) as accurate representation of the actual flight.

7.2 The landing

The figure 7.3 shows the output of the algorithm for the landing phase of the flight number 1. The data starts with zero output as the airplane flies too high for the radar sensor to measure it. Then the radar sensor starts picking up response from the ground. The change of the outputted data from zero to measured height is not imminent, though. That is because of the averaging described in section 6.2. The averaging outputs smoother and more „trustworthy“ data as it prevents occasional peaks in output, but it causes problems when there is a legitimate imminent big change of the measured height. The problem is also present during the take–off phase as described in previous section. There have been

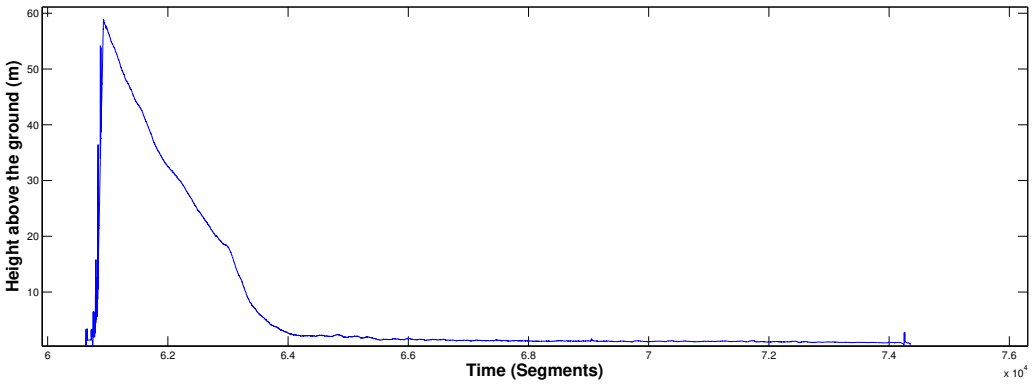

Figure 7.3: The landing phase of the flight number 1.

efforts to address this problem, but none of them was robust and usually „damaged“ the outputted data also in other parts of the flight.

Nonetheless, after this transition period the algorithm starts outputing accurate data, as the steady descent representing the final approach (see section 2.4 for detailed description) can be seen in the figure.

After the final approach, the height begins to stabilize approximately at 3 metres and the descent continues with much smaller intensity. This is called the round–out and/or flare and is described in section 2.4.

The actual touchdown (section 2.4 is not clearly visible in the data, but most probably happens when the height stabilizes around the 1 metre. The exact location may be near the small „bump“ in the data between the 6.8 and 7 marks or near the 7.4 mark on the x–axis. This „bump“ may indicate the small jump of the airplane immediately after the first touchdown as a result of the spring effect of the landing gear. After that, the height is more or less stable at the same value as before the take–off. Near the end of the data there is again a phase where the data are rather unstable and oscillate between very weak response considered as noise and occasional frequency and amplitude peaks just like before the take–off. This was discussed in the previous section.

Again, even though there is no ground–truth reference to verify the output, the data correspond to the standard landing manoeuvre of the light airplane and therefore could be considered as trustworthy.

7.3 The flight number 2

The flight number 2 is very similar to the flight number 1. However, there is one interesting difference during the take–off phase. Because of this and also for completeness sake, the results for this second flight are also provided in the same manner as for the flight number 1. The figure 7.4 shows the whole flight number 2, whilst the figures 7.5 and 7.6 show the take–off phase and the landing phase, respectively.

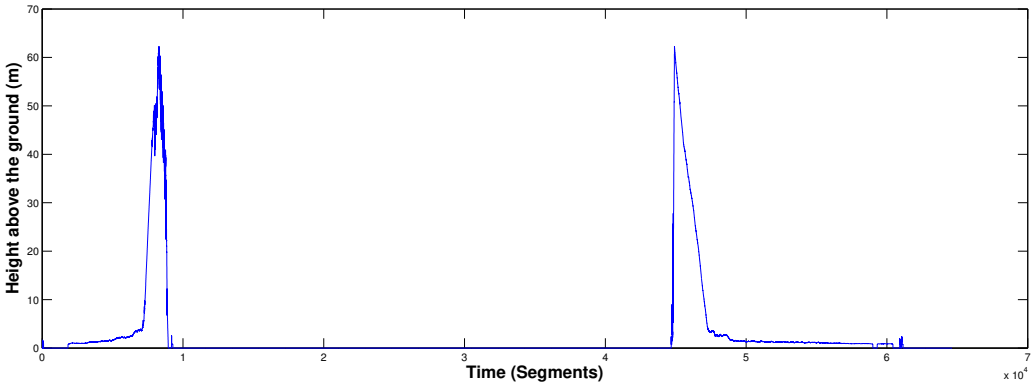

Figure 7.4: The flight number 2.

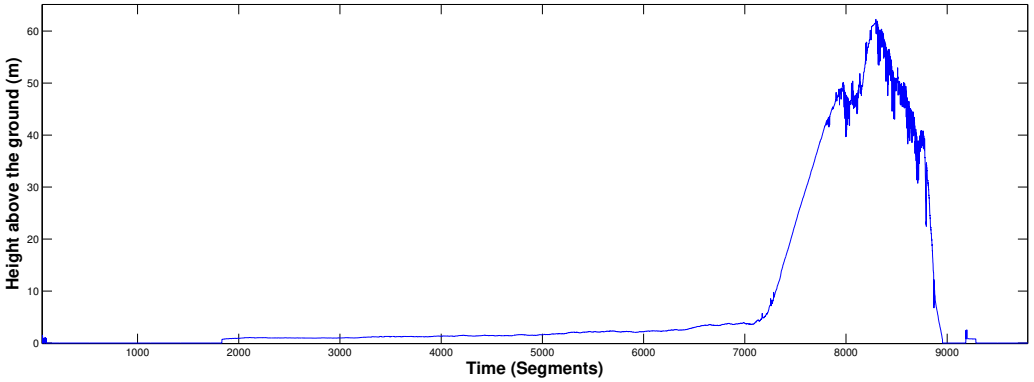

Figure 7.5: The take–off phase of the flight number 2

The take–off

The main difference is in the take–off phase (the figure 7.5).From the start, the phase can be seen, where the response was rather unstable and under the threshold so the algorithm outputs zero.

After this, the radar starts picking up the response and outputs the same height as in the flight number 1. This height starts to increase, indicating that the aicraft took–off and maintains a low–level flight in order to gain enough airspeed to begin initial climb.

After a while, a rapid yet steady climb can be seen in the data, corresponding to the airplane reaching sufficient airspeed and climbing after taking–off. There, the main difference between the flight number 1 and the flight number 2 in terms of the radar response and subsequently outputted height occurs.

The response for the high ranges was much more unstable in this flight and began to appear and disappear between the frames, causing the output to take much more time to drop to zero (as the averaging is used) and making the output incorrect. The frequency of occurrence of this high–frequency peak drops steadily after reaching the maximum height, but is frequent enough to „spoil“ the outputted data.

Even after dropping to zero there is a small non–zero output caused by the response appearing in the data once again. This is the biggest weakness of this algorithm. It could

be addressed by further fine–tuning of the parameters should more data are available in the future or developing a robust detection method for such situation. A one possible method how to deal with this situation would be to limit the maximum height to „safe“ value where the response is stable and stop measurement there. Looking at the outputted data from the flight number 1, this limit would be around $40\,m$.

Fortunately, the main goal of the whole thesis was to develop the algorithm aimed at the landing phase of the flight, which looks reasonable for both the flight number 1 and flight number 2.

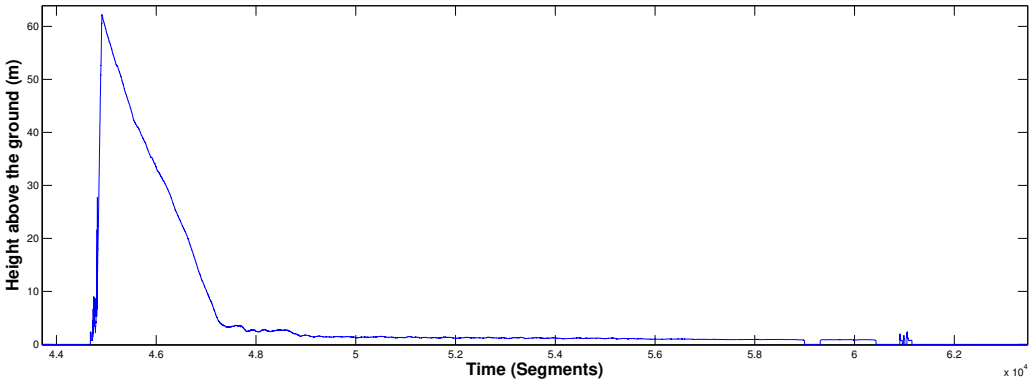

Figure 7.6: The take–off phase of the flight number 2.

The landing

The landing phase is rather similar to the landing phase of the flight number 1. The maximum detected height was almost the same as in the flight number 1. The steady descent is again clearly visible in the data.

The difference is that the height was stabilized faster during the round–out, indicating stronger pilot input on the yoke pitch axis suggesting that the airplane has descended faster than he estimated or initiated the descent too far from the runway.

However, there are even two steps visible in the data. The first round–out and then slight descent and again stabilized height (second round–out). This could indicate that the first round–out was performed too fast and stabilized the airplane too high. Of course, the combination of this and too steep descent or descent initiated too far from the airfield is also possible.

After this, the height continues as expected, with a slight descent around the 49 000 mark, which could be the touchdown or the final positioning of the airplane above the runway and subsequent wait for the touchdown as the airspeed decreases.

Summary

The following conclusion can be drawn from the achieved results:

- The minimum detectable height is $1\,m$.
- The maximum detectable height is up to $62\,m$.

- The algorithm performed well for both landing phases, which was the main goal of this thesis.
- The used averaging causes certain „delay“ in the outputted data. More tests and comparison with the reference height are needed to determine the best averaging window.
- The algorithm behaved incorrectly during the take–off phase of the flight number 2 because of the unstable radar response for heights above $40\,m$. The possible solution is discussed in the next chapter.
- The goals about minimum and maximum detectable height were achieved

With these findings in mind, the results can be deemed satisfactory with the room for improvement. The possible changes and improvements are discussed in more detail in the next chapter.

Chapter 8

Potential future work, improvements and usage

Even though the achieved results are satisfactory, there is still a room for improvements and/or changes, especially with the fact that the ultimate goal of this thesis is to develop the algorithm which would be usable in real–world commercial product in mind. And not only usable, but also performing well in terms of accurate results and the robustness.

The possible future improvements include:

- The current algorithm relies on several parameters, which were tuned with respect to the available data. This data were provided without much description about the general conditions during the data acquisition, such as the mounting height of the radar module, the surface, from which the radar waves were reflected (grass, concrete, asphalt, ...), weather conditions or aicraft position with respect to the ground (mainly the pitch and roll angles, as they affect the angle at which the radar waves are transmitted and received). Nor they were provided with any kind of ground–truth reference for height computation, be it the data from certified radio altimeter, satellite navigation systems or even rough comparison with the pressure altimeter, which every light aircraft is equipped with.

  Unless more data are available, it is not possible to say whether current settings of the algorithm are robust and work in all situations. Further tests and fine–tuning are therefore vital for potential application of the algorithm in the commercial product.

- Evaluating the accuracy of the algorithm. This is closely related to the previous point. No ground–truth data were available, so it is not possible to say with one–hundred percent certainty how accurate are the results, even if they look „trustworthy“. The most ideal comparison would be with the certified radio altimeter, however, any kind of reference data would be helpful, such as data from satellite navigation systems or even pressure altimeter for rough estimation.

- The problem with the averaging when the radar sensor loses response or starts picking up response. Robust solution to this problem would without any doubt enhance the reliability of the output and hence the trustworthiness of the algorithm.

- The problem with the unstable response which currently causes incorrect height output for the take-off phase of the flight number 2. This could be addressed by robust

detection method, but probably the better solution would be to compute (and output) only „safe“ heights where the response is stable. With the data available, this threshold would be set around the 40 to 42 m, which still satisfies the requirement for detectable height. This would represent a trade–off between the maximum detectable height and trustworthiness of the outputted data. As the response for the landing phase has been stable even for heights around 62 m, it would be sensible to introduce this limit only for the take–off phase. This has been experimented with, but even though there have been some improvements during the take–off phase, the solution worsened the output for the landing phase, which has the higher priority.

The potential usage of the developed algorithm is in the radio altimeter of the light aircraft even though it may be possible to use it also for other general purposes of height/range measurement, such as the measurement of liquid level in tank or possibly as a forward–looking radar in car (adaptive cruise–control, automatic braking systems). However, this is purely hypothetical and would need to be verified using the real–world data as they may be rather different from the data acquired during the flight of the airplane.

To achieve this, the algorithm needs to be transferred from Matlab code/environment to the C/C++ form able to run on the System–on–chip devices, such as Xilinx Zynq. Of course, the improvements mentioned earlier would be help the case.

After the implementation in C/C++, it would be also possible to evaluate the performance on the selected target platform and possible change it, whether to use the device with more computational power to safeguard the smooth performance of the algorithm or to use device with less computational power, which are generally cheaper to reduce the cost of the final commercial product.

This thesis, or, to say it better, this effort to create the radio altimeter, could even be a starting point for future Bachelor's or Master's thesis.

For example, currently the idea how to provide the pilot with these vital information is to use the sound signalling (be it the change of pitch of the sound or the frequency of „beeping“ or even the combination). However, the common way how to display this data to pilot is of course visual, which could mean displaying the digital number or displaying the virtual gauge of the altimeter. Seeing the rapid development and advancement in car industry and mobile devices, it may be interesting to explore the possibilities of displaying this information using smartphones, tablets, head-up displays or creating the dedicated airplane dashboard to display all kinds of information for pilot.

As it was already mentioned several times, the goal is to create the working radio altimeter. The radar signal processing algorithm is only one component of such system, the other one being the hardware which would control the radar module. This component is currently being developed using the Xilinx Zynq SoC as a thesis of another student. The results of these two thesis „connected“ could create a viable solution and, together with the radar sensor, be a part of final commercial product: a radio altimeter for the light aircraft.

Chapter 9

Conclusion

The goal of this Master's thesis was to design and implement an algorithm for radar signal processing for radio altimeter, which could be used as an altimeter in the light aircraft, especially for the landing manoeuvre. The algorithm was to be as simple as possible so as to ensure the performance on the reasonably priced embedded system.

The design and subsequent implementation of the algorithm were successful with the results being satisfactory.

The work, which was carried out could be divided in to two parts. The first part consisted of the research work about the height measurements devices used in aviation, the landing phase of the flight of the light aircraft, radar principle of operation and radar types, radar signal processing and digital signal processing in general. This work is summarized in the first four chapters. Based on this work a proposal of solution is described in the next chapter.

The second part was the design and implementation of the algorithm itself and evaluation of the achieved results. Of course, the achieved results and their evaluation invoked the changes in the design and implementation forming the iterative process. The data used for testing the algorithm were captured during the real flight of the light airplane. Because of this, the data included noise or unstable radar response which made the process of extracting the useful information non–trivial, but the changes to the algorithm and implementation continued until the results were satisfactory. The goals of detecting the minimum and maximum heights have been achieved with the minimum detectable height being $1\,m$ and the maximum detectable height around $62\,m$

The achieved results in form of the computed height above the ground of the airplane could not be verified against the ground–truth reference, but they correspond to the expected output based on the knowledge of the light airplane flight phases.

The future of this project lies primarily in acquisition of more real–flight data and subsequent tests of the algorithm (and possible fine–tuning of it) as well as implementation on the embedded system with the ultimate goal of introducing the radio altimeter for the light aicraft to the market as a commercial product in the cooperation with the industry.

Bibliography

[1] Meter Gives Elevation. *Popular Science. New York: Popular Science Publishing Co. Inc.*. vol. 118, no. 3. March 1931.

[2] Standard Atmosphere. ISO 2533-1975. Geneva: International Organization for Standardization. 1975.

[3] Quantization. Natick: The MathWorks, Inc. 1994-2017. [Online; visited 2017-05-12]. Retrieved from: https://www.mathworks.com/help/comm/ug/quantization.html

[4] *Theoretical Knowledge Manual for ATPL: Aircraft General Knowledge 4 (022)*. Frankfurt: Jeppesen GmbH. second edition. 2002. ISBN 0-88487-285-8.

[5] *Theoretical Knowledge Manual for ATPL: Navigation 2(060 062)*. Frankfurt: Jeppesen GmbH. second edition. 2002. ISBN 0-88487-285-8.

[6] IVS-948. Donnersdorf: InnoSenT GmbH. 2014. [Online; visited 2016-05-06]. Retrieved from: http://www.innosent.de/fileadmin/media/dokumente/datasheets/IVS-948.pdf

[7] Standard Products. Donnersdorf: InnoSenT GmbH. 2014. [Online; visited 2016-05-06]. Retrieved from: http://www.innosent.de/fileadmin/media/dokumente/Downloads/InnoSenT_Standard_Products_web.pdf

[8] *Airplane Flying Handbook*. Washington, DC: U.S. Department of Transportation. 2016. FAA-H-8083-38. Retrieved from: https://www.faa.gov/regulations_policies/handbooks_manuals/aviation/airplane_handbook/

[9] Zynq-7000 All Programmable SoC. San Jose: Xilinx Inc. 2016. [Online; visited 2016-01-08]. Retrieved from: https://www.xilinx.com/support/documentation/product-briefs/zynq-7000-product-brief.pdf

[10] MATLAB - Overview. Hyderabad: Tutorials Point. 2017. [Online;visited 2016-01-08]. Retrieved from: https://www.tutorialspoint.com/matlab/matlab_overview.htm

[11] Amos, J.: EU's Galileo satellite system goes live after 17 years, London: BBC. 2016. [Online; visited 2016-12-23]. Retrieved from: http://www.bbc.com/news/science-environment-38329341

[12] Borgelt, M.: GPS Altitude vs Pressure Altitude. Toowoomba: Borgelt Instruments. 2011. [Online; visited 2016-12-23].
Retrieved from:
http://www.borgeltinstruments.com/GPSvsPressurealtitude.pdf

[13] Černocký, J.: Zpracování řečových signálů — studijní opora. Brno: Brno University of Technology. 2006.
Retrieved from:
http://www.fit.vutbr.cz/study/courses/ZRE/public/opora/zre_opora.pdf

[14] Houcque, D.: Introduction to MATLAB for engineering students. Evanston: Northwestern University. 2005. [Online; visited 2016-01-08].
Retrieved from: http://www.mccormick.northwestern.edu/documents/students/undergraduate/introduction-to-matlab.pdf

[15] Kdér, F.; et al.: *Učebnice sportovního letce*. Praha: Naše Vojsko. second edition. 1980.

[16] Komarov, I. V.; Smolskiy, S. M.: *Fundamentals of Short–range FM radar*. London: Artech House. 2003. ISBN 978-1580531108.

[17] Maršík, L.: *Algorithms for signal processing in FPGA*. Master's Thesis. Brno: Brno University of Technology. 2010.

[18] Oppenheim, A. V.; Schafer, R. W.: *Discrete-Time Signal Processing*. Upper Saddle River: Prentice Hall. second edition. 1999. ISBN 0-13-754920-2.

[19] Scholten, U.: Radar Principle. Iserlohn: SkyRadar. 2008-2017. [Online; visited 2016-12-27].
Retrieved from: http://www.skyradar.com/radar-basics/radar-principle/

[20] Skolnik, M.: *Radar Handbook*. USA: The McGraw-Hill Companies. third edition. 2008. ISBN 978-0-07-148547-0.

[21] Skolnik, M.: Radar. Chicago: Encyclopædia Britannica Inc.. 2015. [Online; visited 2016-12-04].
Retrieved from: https://www.britannica.com/technology/radar

[22] Wojtkiewicz, A.; Misiurewicz, J.; Nałecz, M.; et al.: Two-dimensional signal processing in FMCW radars. In *Proc. XXth KKTOiUE*. Poland. 1997. pp. 475–480.

[23] Wolff, C.: Doppler–Effect. Germany: Christian Wolff. 1998. [Online; visited 2016-12-27].
Retrieved from: http://www.radartutorial.eu/11.coherent/co06.en.html

[24] Wolff, C.: Frequency–Modulated Continuous–Wave Radar (FMCW Radar). Germany: Christian Wolff. 1998. [Online; visited 2016-12-27].
Retrieved from: http://www.radartutorial.eu/02.basics/Frequency%20Modulated%20Continuous%20Wave%20Radar.en.html

Appendix A

Content of the DVD

An enclosed DVD disc contains the following:

- this document in `pdf` format.
- `latex` source files of this document.
- *Matlab* file which contains the implementation of the work with the two test data files included.
- `README` file with detailed description of the DVD content and the usage of the *Matlab* script.